Tampere University

Amna Music

DECORATION OF NOROVIRUS-LIKE PARTICLES WITH CORONAVIRUS (SARS-COV-2) ANTIGENS TO CREATE POTENTIAL VACCINE CANDIDATE

Faculty of Medicine and Health Technology
Master´s thesis
April 2021

ABSTRACT

MUSIC AMNA: Decoration of norovirus-like particles with coronavirus (SARS-CoV-2) antigens to create potential vaccine candidate
Master´s thesis
Tampere University
Master's Programme in Biomedical Technology
April 2021

Background and aims: Pathogens that can cause severe epidemic/pandemic outbreaks, like the current coronavirus (SARS-CoV-2), have the potential to inflict deleterious effects on a global level. In this project, we aimed to create a modular and fast-to-produce vaccine platform based on norovirus-like particles. We wanted to address the potential challenge of a previously developed SpyCatcher/SpyTag noroVLP platform by utilizing a similar three-part SnoopLigase system to decorate noroVLPs with SARS-CoV-2 antigens. Both methods are based on the formation of isopeptide bonds between peptide tags that can be fused with antigens. In this project receptor-binding domain (RBD) and receptor-binding motif (RBM) of SARS-CoV-2 were fused to SnoopTagJr tag and DogTag was expressed on the surface of noroVLP. SnoopLigase was used to form a bond between respective tags and generate potential vaccine candidates against SARS-CoV-2.

Materials and methods: SnoopLigase was expressed in *E. coli* BL21(DE3) Star cell line. The DogTag-noroVLPs and HisTag-SnoopTagJr-RBD were produced using the baculovirus-insect cells expression system. SnoopTagJr-RBM was chemically synthesized by a commercial provider. SnoopLigase and SnoopTagJr-RBD were purified with Affinity Chromatography. Purified SnoopLigase was biotinylated both chemically and enzymatically. The DogTag-noroVLPs were first purified with sucrose-gradient centrifugation and then polished with Ion Exchange Chromatography. SDS-PAGE and Western Blotting were utilized for purity assessment and characterization. Conjugation between DogTag-noroVLPs and SnoopTagJr-SARS-CoV-2 antigens was catalysed with SnoopLigase in the different onset of conditions. Dynamic light scattering, Differential scanning calorimetry, and Transmission electron microscopy were used to assess the homogeneity, stability, and morphology of particles.

Results: The SnoopLigase production was successful, with a high purity sample and great yield of 20 mg/L. Both enzymatic and chemical biotinylation of SnoopLigase was accomplished. The DogTag-noroVLPs production in Hi5 insect cells and two-step purification resulted in 90% pure particles with a yield of 16 mg/L. The size of DogTag-noroVLPs was estimated to be ~58 nm and the Tm of 64 °C. The particles were stable for one month at +4 °C. SnoopTagJr-RBD was produced similarly, however, the production yield was 6 mg/L and purity ~80%. SnoopLigase was efficient in forming the conjugation complex between DogTag-noroVLPs and SnoopTagJr-antigens. Differently biotinylated SnoopLigase has shown the same results. Control reactions were able to confirm the efficiency of SnoopLigase to form conjugates. Removal of the SnoopLigase from the end-product was not successful and requires additional optimization and trials.

Conclusion: Decoration of the norovirus-like particles with SARS-CoV-2 antigens by SnoopLigase system was successful. The SnoopTagJr-RBD production needs optimization to obtain a higher yield. The long-term storage of DogTag-noroVLPs should be explored in further research. Removal of the SnoopLigase requires certain adjustments and the stability of conjugated particles needs to be measured before pre-clinical trials. However, with a couple of modifications, this vaccine platform has plenty of potential for future application in vaccine development.

Keywords: norovirus, virus-like particle (VLP), SARS-CoV-2, antigens, vaccine, SnoopLigase, biotinylation, decoration

PREFACE

This Master´s thesis project was conducted in the Protein Dynamics research group in the Faculty of Medicine and Health Technology, Tampere University.

I would like to express my gratitude towards people that contributed to this project directly and indirectly. Special and massive thanks to Professor Vesa Hytönen for the opportunity to work in this field of research and for giving me immense support and understanding. I couldn´t ask for a better teacher and boss. I also want to thank my supervisor, MSc Vili Lampinen for arranging this project and helping me with the lab work and thesis writing.

I would like to thank everybody in our lab, for support and a good atmosphere. Huge thanks to Ph.D. Minna Hankaniemi for helping me always with my experiments and technical issues, even though she was busy with her work. Special gratitude goes to amazing laboratory technicians Ulla Kiiskinen, Niklas Kähkönen, and Merja Jokela for all the guidance, tips, and help they provided me during my work.

I´m grateful the most to my parents and family because without their selfless support I would not be here today. Also, a big thanks to Dado and my friends for their support and encouragement.

Tampere, April 2021

Amna Music

CONTENTS

1. INTRODUCTION 1
2. LITERATURE REVIEW 3
2.1 Coronavirus 3
2.1.1 General overview on coronaviruses 3
2.1.2 SARS-CoV-2 genome and structure 4
2.1.3 Infection and host immune response 6
2.2 Virus-like particles 9
2.2.1 Overview and applications 9
2.3 Decoration of VLPs 10
2.3.1 SpyCatcher/SpyTag system: principles 11
2.3.2 SnoopLigase system 12
2.4 Vaccines and immunity: 14
2.4.1 Virus-like particles vaccines 14
2.4.2 SARS-CoV-2 vaccines 15
3. OBJECTIVES 18
4. MATERIALS AND METHODS 19
4.1 Main methods 19
4.1.1 SDS-PAGE and Western blot: 19
4.1.2 Chromatography methods: 20
4.1.3 Insect cells 21
4.1.4 Baculovirus stock productions 21
4.1.5 Titration of recombinant baculovirus stocks 23
4.2 SnoopLigase 23
4.2.1 Plasmid amplification and extraction 23
4.2.2 SnoopLigase production: 24
4.2.3 SnoopLigase purification and characterization 25
4.2.4 Chemical biotinylation: 26
4.2.5 Enzymatic biotinylation: 27
4.3 DogTag-norovirus-like particles 27
4.3.1 Plasmid preparation and amplification 27
4.3.2 DogTag-noroVLP production 28
4.3.3 Purification using sucrose density gradient centrifugation 28
4.3.4 Ion Exchange Chromatography 28
4.3.5 Size, homogeneity, and stability measurements 29
4.4 Coronavirus antigens fused with SnoopTagJr 30
4.4.1 Construct design 30
4.4.2 SnoopTagJr-RBD production 30
4.4.3 SnoopTagJr-RBD purification 31
4.5 Conjugation reactions 31
4.5.1 Evaluation of conjugation rate 32
4.5.2 Removal of SnoopLigase 32
5. RESULTS 34

5.1 SnoopLigase 34
5.1.1 Production, purification, and characterization of SnoopLigase 34
5.1.2 Biotinylation of SnoopLigase 36
5.2 Titration of recombinant baculovirus stocks 37
5.3 DogTag-norovirus-like particles 38
5.3.1 DogTag-noroVLP production 38
5.3.2 Purification of DogTag-noroVLPs 39
5.3.3 Size, homogeneity, and stability measurements 40
5.4 Coronavirus antigens fused with SnoopTagJr 41
5.4.1 Production of SnoopTagJr-antigens 41
5.4.2 SnoopTagJr-RBD purification 42
5.5 Conjugation reactions 43
5.5.1 DogTag-noroVLP and 5FAM-SnoopTagJr-RBM 44
5.5.2 DogTag-noroVLP and SnoopTagJr-RBD 46
5.5.3 Control reactions 47
5.5.4 Removal of the SnoopLigase 48
6. DISCUSSION 50
6.1 SnoopLigase 50
6.1.1 Biotinylation of SnoopLigase 50
6.2 DogTag-norovirus-like particles 51
6.2.1 Size, homogeneity, and stability 53
6.3 Coronavirus antigens fused with SnoopTagJr 53
6.4 Conjugation reactions 55
6.4.1 DogTag-noroVLP and 5FAM-SnoopTagJr-RBM 55
6.4.2 DogTag-noroVLP and SnoopTagJr-RBD 55
6.4.3 Control reaction 56
6.4.4 Removal of the SnoopLigase 56
6.5 Other perspectives 57
7. CONCLUSION 59
8. REFERENCES 60
9. APPENDICES: AMINO ACID SEQUENCES OF DESIGNED PROTEINS 69
9.1 DogTag-noroVLP 69
9.2 SnoopTagJr-RBD 69
9.3 SnoopTagJr-RBM 69

LIST OF SYMBOLS AND ABBREVIATIONS

aa	Amino acid
AcMNPV	*Autographa californica multicapsid nucleopolyhedrovirus*
AEX	Anion exchange chromatography
AH	Aluminum hydroxide
Amp	Ampicillin
APC	Antigen-presenting cells
ARDS	Acute respiratory distress syndrome
ATP	Adenosine triphosphate
BCRs	B cell receptors
BirA	*E. coli* biotin ligase
BSA	Bovine serum albumin
CnaB2	Immunoglobulin-like collagen adhesin domain
CNCA	Charge-neutralized chimeric avidin
CoV	Coronavirus
COVID-19	Coronavirus Disease 2019
DC	Dendritic cells
DLS	Dynamic light scattering
dpi	Days post infection
DSF	Differential scanning fluorometry
ER	Endoplasmic reticulum
FbaB	Fibronectin-binding protein
FBS	Fetal bovine serum
FP	Fusion peptide
gp64	AcMNPV envelope glycoprotein
HABA	4'-hydroxyazobenzene-2-carboxylic acid assay
hACE2	Human angiotensin-converting enzyme 2 receptor
HCoV- HKU1	Human coronavirus HKU1
HCoV-229E	Human coronavirus 229E
HCoV-NL63	Human coronavirus NL63
HCoV-OC43	Human coronavirus OC43
Hi5	*Trichoplusia ni* insect cells
HR1- HR2	Heptad repeats
HRP	Horseradish Peroxidase
IC	Intracellular domain
IEX	Ion exchange chromatography
IFNs	Interferons
IL	Interleukines
IMAC	Immobilized metal affinity chromatography
IPTG	Isopropyl β-D-1-thiogalactopyranoside (an allolactose analog)
IRF3/7	IFN regulatory factors
ISGs	IFN-stimulated genes
LB	Lysogeny broth bacterial growth medium
M2e	Ectodomain of influenza matrix-2 protein
MAVS	Mitochondrial antiviral-signalling
MDA5	Melanoma differentiation-associated protein 5

MERS-CoV	Middle East respiratory syndrome coronavirus
MHC	Major histocompatibility complex
MOI	Multiplicity of infection
MyD88	Myeloid differentiation primary response 88
NF-kB	Nuclear factor-κB
NHS	N-Hydroxysuccinimide
Ni-NTA	Nickel-nitrilotriacetic acid
NKRF	NF-κB repressing factor
NLRP3	NLR family pyrin domain containing 3
NoroVLP	Norovirus-like particle
Nsps	Non-structural proteins
O/n	Overnight
OD	Optical density
ORFs	Open reading frames
PBS	Phosphate-buffered saline
PFU	Plaque forming units
PRRs	Pathogen recognition receptors
PTMs	Post-translational modifications
RBD	Receptor-binding domain
RBM	Receptor-binding motif
RIG-I	Retinoic acid-inducible type I
RNP	Riboncleocapsid
RT	Room temperature
SARS-CoV-1	Severe acute respiratory syndrome coronavirus 1
SARS-CoV-2	Severe acute respiratory syndrome coronavirus 2
SD1-SD2	Subdomains
SDS-PAGE	Sodium dodecyl sulphate polyacrylamide gel electrophoresis
Sf9	*Spodoptera frugiperda* insect cells
sgRNA	Subgenomic RNA
SM	Starting material
SOC	Super optimal broth medium
SOP	Standard operating procedure
Spy-noroVLP	SpyTagged norovirus-like particle
ssRNA	Positive single-stranded RNA
TBS	Tris-buffered saline
TE-buffer	Tris-EDTA (ethylenediamine tetra-acetic acid) buffer
TEM	Transmission electron microscopy
TLR8-TLR9	Toll-like receptors
TM	Transmembrane region
TMH1-TMH3	Terminal transmembrane helices
TMPRSS2	Transmembrane serine protease enzyme
TNF	Tumour necrosis factors
UTR	Untranslated region
WB	Western blotting
VLP	Virus-like particle

.

1. INTRODUCTION

We are currently experiencing a worldwide pandemic due to the emergence of the SARS-CoV-2 virus in late 2019. The SARS-CoV-2 virus is a member of the group of coronaviruses, responsible for severe outbreaks throughout history [1]. Until now, over 130 million infections have been confirmed and more than 2.8 million were fatal [2]. Pandemics and epidemics of infectious diseases are occurring more often over the past century, increasing mortality and morbidity in a wide geographical area, causing noted damage to global politics and the economy, as well as on social life. The causes for the elevated likelihood of pandemic are correlated with rapid urbanization, exploitation of natural resources, global migrations and integrations [3].

One of the most effective ways to fight and tackle infectious pathogens is the development of vaccines that can protect us against them [4]. Therefore, the generation of a modular and fast-to-produce vaccine platform that can efficiently adapt to pathogen changes is essential. One of the safest and most efficient ways to achieve this is the utilization of virus-like particles (VLPs). VLPs are empty particles formed from the viral structural proteins without genomic material, making them safe and non-infectious. Their morphology enables them to elicit strong cellular and humoral immune responses. Rapid production is possible under optimized conditions as well as the surface decoration with antigens to exhibit a robust and specific immune response which makes them a powerful tool in vaccine research and development [5,6]. One of the methods for faster and modular decoration of VLPs is based on SpyCatcher/SpyTag [7] and SnoopLigase system [8], which utilize a peptide (protein) – peptide ligation approach. Both systems consist of peptide tags that can be fused with VLPs and desired antigens that get linked together via isopeptide bonds. This system provides cost-efficient mass production that can be easily modified and adapted to variations in antigen structure [9].

Protein Dynamic research group has established a modular VLP vaccine platform based on the norovirus-like particles (noroVLPs). The noroVLPs were decorated with influenza antigens via SpyCatcher/SpyTag system and used in pre-clinical trials [10]. The potential downside of this platform is the size of the SpyCatcher protein that stays as a part of the end-product. In this study, we were aiming to construct new noroVLPs, in which we

utilized a similar SnoopLigase system that enables the removal of SnoopLigase from the conjugation complex and can overcome the challenge of the SpyCatcher system. The final goal was to create an accessible and modular vaccine platform that can respond to emerging pandemics, like the current coronavirus outbreak.

2. LITERATURE REVIEW

2.1 Coronavirus

2.1.1 General overview on coronaviruses

Coronaviruses are a highly diverse group of viruses, that contain a positive single-stranded RNA (+ssRNA) and viral envelope. The family *Coronaviridae* belongs to the suborder *Coronavirineae* and the order *Nidovirales* [11]. The first infections with coronaviruses have been found in domestic chickens in North America in the 1920s. Coronaviruses that infect humans, described in the 1960s, were causing infections of the upper respiratory tract in children. Since then, several other different human coronaviruses have been characterized and continuous research has provided an insight into their epidemiology [12]. It is known that these viruses can infect humans, other mammals, and birds, and that the transmission from animals to humans is possible. This represents an additional challenge for controlling and preventing infections. There are four subspecies of coronaviruses: alpha, beta, gamma, and delta coronaviruses, of which the alpha and beta groups infect humans and mammals [13,14]. The infection can result in mild (common cold) to severe outcomes that include lung damage and death. The four endemic types of coronaviruses that infect humans are known to cause generally mild symptoms: HCoV-NL63, HCoV-229E (both α-CoV), HCoV- HKU1, and HCoV-OC43 (both β-CoV) [15].

The recently emerged coronavirus SARS-CoV-2 responsible for the ongoing worldwide pandemic was initially discovered in late 2019 in Wuhan (China) [16]. This virus is part of the β-coronaviruses group together with the Severe acute respiratory syndrome coronavirus 1 (SARS-CoV-1) and Middle East respiratory syndrome coronavirus (MERS-CoV) responsible for severe outbreaks in 2003 and 2012 respectively [17]. All three of them are highly pathogenic zoonotic viruses that originated from the bats. The intermediate host for MERS-CoV transmission to humans was dromedary camels, while for SARS-CoV-1 were civets and raccoons [18,19]. The intermediate host for SARS-CoV-2 is not determined yet and the topic is still under extensive research. The SARS-CoV-2 exhibits a higher infectivity rate due to increased affinity towards receptor in comparison to SARS-CoV-1 and MERS-CoV, but lower fatality [20]. The common feature of these viruses is the presence of an envelope spike glycoprotein (S) that protrudes

from viral capsid making the virus particle resemble ´´crown´´ under the electron microscope, hence the name corona (*lat.* crown) [14].

2.1.2 SARS-CoV-2 genome and structure

Using the sequence alignment methods, it has been determined that the SARS-CoV-2 shares ~80% of sequence homology with SARS-CoV-1 and ~50% with MERS-CoV [21]. The genome of SARS-CoV-2 consists of ~30kb, which includes 14 open reading frames (ORFs) encoding for more than 20 different proteins (Figure 1). The replication complex composed of ORF1a and ORF1b is located downstream of the 5´utranslated region (UTR). The pp1a polyprotein (ORF1a) contains ten non-structural proteins (nsps) while the pp1ab polyprotein (ORF1b) includes 16 nsps [17]. These proteins form a replication complex by the process of autoproteolysis. Four genes encoding structural proteins are distributed near the 3´untranslated region, with eight accessory genes in-between whose function is not yet clarified [22].

Four structural proteins are required for the assembly of viral particles: nucleocapsid (N), membrane (M), envelope (E), and spike glycoprotein (S) [23]. The SARS-CoV-2 particle has a double-layer lipid envelope and a diameter range of 50-200 nm [24] (Figure 1). The nucleocapsid protein is responsible for packing the viral RNA into spiral ribonucleocapsid (RNP) and participates in genome encapsulation through interaction with other structural proteins during virion assembly. It also plays a pivotal role in virus replication, transcription, and translation processes [25]. The M and E proteins, which are highly conserved among the β-coronavirus group, play a major role in the modulation of virion assembly. The M protein contains the N hydrophilic, cytoplasmic, and transmembrane (TMH1-TMH3) domains. Through interactions with itself and other proteins, it initiates membrane budding and enhances the formation of new virions [26].

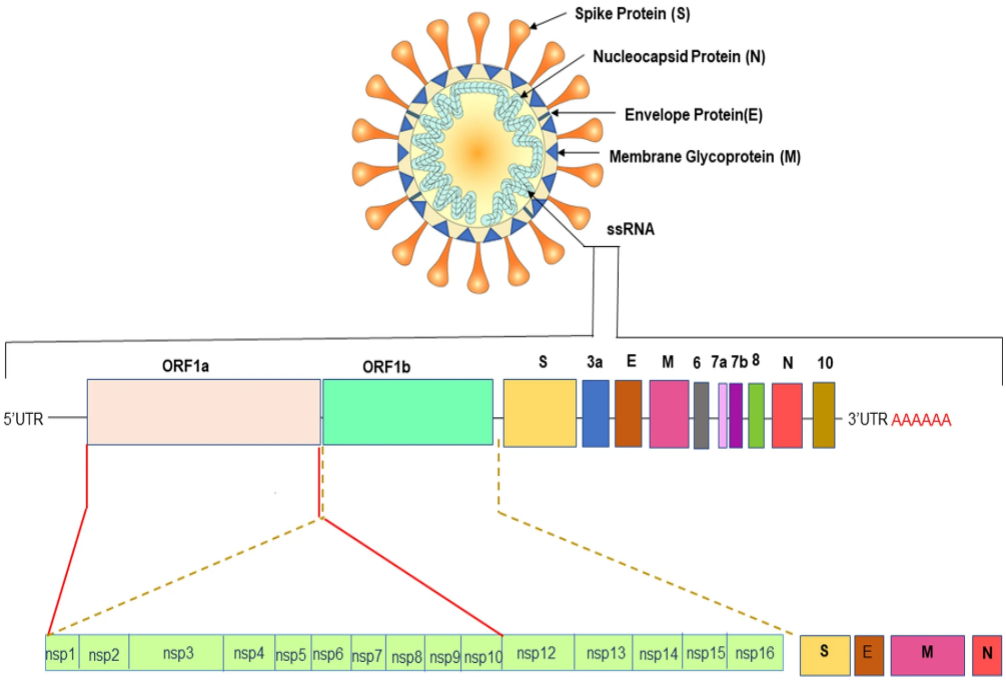

Figure 1. *Schematic overview of SARS-CoV-2 particle and genome structure. Four structural proteins are responsible for the assembly of helical viral particle: spike (S) glycoprotein, membrane (M), envelope (E) and nucleocapsid (N) protein. The RNA genome is packed into ribonucleocapsid and it consists of replicase complex (ORF1a and ORF1b), genes encoding for structural proteins and accessory genes. ORF1a encodes for polyprotein pp1a that contains 10 non-structural proteins (nsp1-nsp10) and ORF1b encodes for pp1ab that has 16 non-structural proteins (nsp1-nsp16). Adapted from* [27].

The E protein also has three domains: The N hydrophilic, transmembrane, and long C-terminal domains. This protein plays a role in pathogenesis through interactions with host junction proteins which promote the spread of the virus to other tissues [28]. The transmembrane spike (S) glycoprotein assembles into trimers on the virus surface and mediates the entry into host cells. The Spike protein is divided into S1 and S2 subunits. The S1 subunit contains a receptor-binding domain (RBD) that can recognize and bind to human angiotensin-converting enzyme 2 receptor (hACE2) [29,30]. The major functional domain of the RBD is the receptor-binding motif (RBM) which enables connection to the receptor and stability of the whole RBD domain [31] (Figure 2B). The S2 subunit induces the fusion of viral particles into the host cell membrane [32], and can exist in prefusion and postfusion conformation. It consists of four regions: a fusion peptide (FP), transmembrane region, and two heptad repeats (HR1 and HR2) [33] (Figure 2A). The sequence homology between Spike protein of SARS-CoV-2 and SARS-CoV-1 is 77%, (RBD ~74%, and RBM ~50%), indicating highly conserved regions and potential vaccine targets [31]. The SARS-CoV-2 (and other CoVs) have a lower mutation rate due to the presence of RNA-proofreading enzymes (exoribonuclease domain in nsp14 protein) [34] which is usually not found in other RNA viruses.

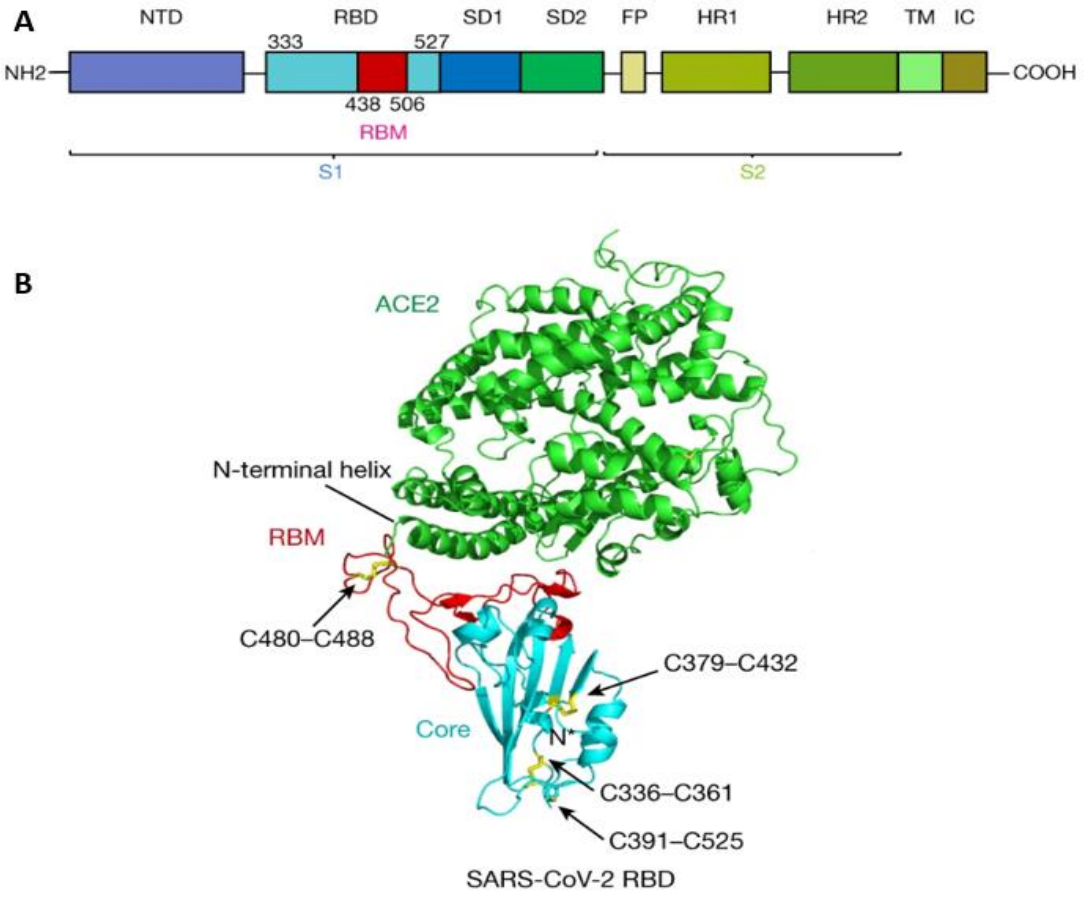

Figure 2. *SARS-CoV-2 Spike glycoprotein gene rearrangement and structure of RBD domain bound to hACE2 receptor.* ***A)*** *Spike glycoprotein regions: N-terminal domain (NTD); RBD with RBM; SD1 and SD2 subdomains; fusion peptide (FP); HR1 and HR2 heptad repeats; transmembrane region (TM) and intracellular domain (IC).* ***B)*** *The SARS-CoV-2 RBD domain bound to ACE2 (showed in green). The core of the RBD domain is shown in the cyan and RBM domain in red. The N-terminal domain of the ACE2 receptor that binds to RBD is indicated. Sticks and arrows represent a disulfide bond in the RBD domain. Modified from* [30].

2.1.3 Infection and host immune response

SARS-CoV-2 is primarily transmitted directly or indirectly via infectious respiratory droplets. The main target of the virus in humans is the epithelial cells of the respiratory tract. The SARS-CoV-2 virus can also be transferred from contaminated surfaces through the mucous of the eyes, nose, and mouth [35]. The virus causes a Coronavirus Disease 2019 (COVID-19) with a majority of people having mild symptoms (headache, fever, cough, lack of smell and taste) or no symptoms (asymptomatic), while some people develop serious clinical manifestation [36]. Many different factors can contribute to disease severity, like viral load, underlying health issues (diabetes, hypertension, malignancy), age, and obesity [35].

As mentioned earlier, SARS-CoV-2 binds to the ACE2 receptor with Spike glycoprotein [32]. The ACE2 is an enzyme expressed on the cell surface of various organs, including lungs, nasopharynx, oral and nasal mucosa, kidney, brain, gastrointestinal tract, etc. [37]. Upon binding to the target receptor, spike protein undergoes proteolytical processing by host proteases which is a crucial step for infection. First, furin protease cleaves S protein between S1 and S2 subunits (S1/S2 site) [38]. Furin-cleavage site (amino acid sequence RRAR) is a unique feature of SARS-CoV-2 since it is not present in MERS-CoV and SARS-CoV-1, and it can explain increased transmissibility rate and viral tropism [38]. Second proteolytical processing involves transmembrane serine protease enzyme (TMPRSS2) that cleaves S2 subunit at S2´ site revealing internal fusion peptide. The viral envelope then fuses with the alveolar cell membrane and the virion is taken up inside the cell by endocytosis or via virus-host membrane fusion [39]. The +ssRNA is released in the cytoplasm of the host cell and gets translated into non-structural proteins (nsps) from ORF1a and ORF1b. The RNA-dependent RNA polymerase also known as nsp12 [40] initiates replication of the viral genome generating -ssRNA template for synthesis of +ssRNA and subgenomic RNAs (sgRNA) that codes for structural proteins. The +ssRNA and structural proteins are trafficked to the Golgi and ER for processing and assembly into new virions. The virions exit cells through exocytosis and infects other cells in the same manner (Figure 3) [23].

The release of SARS-CoV-2 RNA into the host cell activates cellular RNA receptors such as retinoic acid-inducible type I (RIG-I) and the melanoma differentiation-associated protein 5 (MDA5) receptor. They function as pattern recognition receptors (PRRs) and can recognize double-stranded viral RNA [41]. SARS-CoV-2 RNA can also be recognized by endosomal Toll-like receptor 8 (TLR8) and Toll-like receptor 9 (TLR9) that detect viral single-stranded RNA [34]. These receptors recruit myeloid differentiation primary response 88 (MyD88) and mitochondrial antiviral-signalling (MAVS) proteins that induce downstream pathways that activate transcription factors NF-kB and IRF3/7. This results in the generation of pro-inflammatory cytokines (TNF-α, TNF-β, IL-6, IL-8, IL-12, IL-18) and type I interferons (IFN-α and IFN-β) [42]. Type I interferons (IFNs) are essential for controlling viral propagation during early stages of infection. They bind to receptors expressed on various cells like macrophages, inducing the expression of IFN-stimulated genes (ISGs) such as RNAse L and chemokine CXCL10 through STAT/12/IRF9 complex [43]. Furthermore, the virus might activate the NLRP3 (inflammasome sensor), inducing the expression of highly inflammatory cytokine IL-1β that can stimulate pyroptosis like it was detected with SARS-CoV-1 [44]. The secreted cytokines modulate immune response stimulating the recruitment and activation of

macrophages, T and B cells to eliminate the virus (Figure 3). However, the over-expression of cytokines may lead to an unbalanced immune response and hyper-inflammation. The generation of cytokine storms can cause severe clinical symptoms like organ damage that can contribute to acute respiratory distress syndrome (ARDS) and organ dysfunction [24]. The nsp9 and nsp10 proteins can act as mediators for IL-6 / IL-8 signalling through interaction with NF-κB repressing factor (NKRF). That leads to over-activation and recruitment of neutrophils from the periphery [45]. Decreased amount of $CD4^+$ and $CD8^+$ T in peripheral blood (lymphopenia) has been observed in patients with COVID-19 [46] (Figure 3). As a result, there is a strong possibility of secondary bacterial infection which increases the severity of the disease. The role of $CD4^+$ and $CD8^+$ T cells are highly important for the recovery of patients with COVID-19 and the presence of specific $CD8^+$ T cells has been confirmed to aid in the recovery of patients with mild to moderate symptoms [47]. Therefore, one of the goals of vaccine development is to create specific antiviral $CD8^+$ T cells. During SARS-CoV-1 and MERS-CoV infection, the viruses were able to bypass the antiviral response by suppressing type I interferon. Recent studies have shown that SARS-CoV-2 is more susceptible to type I IFN response due to mutations in the ORF3b gene and shortening of the ORF6 gene [48]. The analyses from the immune response of SARS-CoV-2 patients identified the presence of cross-reactive T cells derived from common cold CoVs and SARS-CoV-1 infection that can recognize SARS-CoV-2 [47,49]. This provides promising data for vaccine research development and the generation of long-term immunity.

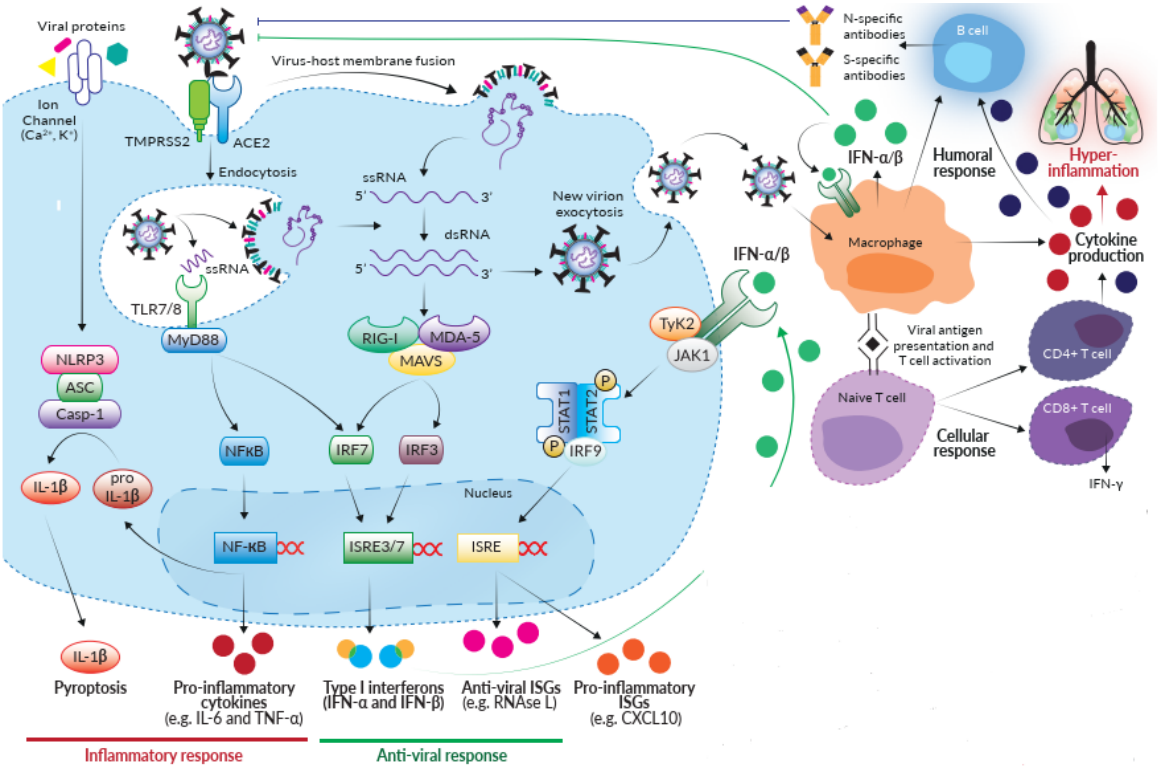

Figure 3. *The SARS-CoV-2 life cycle and predicted host immune response. The SARS-CoV-2 virus binds to the hACE2 receptor on target cells and undergoes proteolytical cleavage by host proteases followed by viral entrance (endocytosis or virus-host membrane fusion). Upon entry into cell virus is detected by RNA (TLR7/8 and RIG-1/MDA-5) and inflammasome sensors (NLRP3). This activates NF-kB and IRF3/7 leading to production of pro-inflammatory molecules (interleukins and type I INFs). The type I INFs also activates expression of IFN-stimulated genes (ISGs) such as RNAse L and chemokine CXCL10. Secreted cytokines regulate immune response by activating and recruiting immune cells. The excessive secretion of cytokines can lead to uncontrolled immune response (hyper-inflammation) and cause severe clinical manifestation. Modified from* [50].

2.2 Virus-like particles

2.2.1 Overview and applications

Virus-like particles (VLPs) are self-assembled empty particles generated from the viral structural proteins (virus surface structures) without genomic material, excluding any possibility of mutation or pathogenic infections [5]. The first discovery of VLP was reported in the 1960s, through the identification of empty viral particles of the hepatic B virus that can also elicit an adequate immune response and thus prevent infection with native hepatic B virus [52]. The development of new technologies and methods has contributed to the further research of VLPs and the discovery of their immense potential in the biomedical world. Up until now, dozens of VLPs have been constructed and derived from different types of viruses [51].

Virus-like particles can be created by removing genetic/infectious material from native viruses or be produced by the heterologous expression of viral structural proteins [53]. Viruses and VLPs contain several properties that give them an advantage over synthetic particles such as their stability, structural symmetry, and uniformity. Their size exists in ranges from 10 - 250 nm, and their 3D structure can be characterized with high-resolution microscopy. Large surface area, the internal cavity, and the high-grade biocompatibility of VLPs enable encapsulation of diverse biomolecules to ensure their transport into specified areas. It is possible to decorate their surface to enhance transportation to targeted cell types or to enhance immune responses [54]. Due to these unique characteristics, VLPs have been extensively utilized in vaccine research and development, as versatile drug/gene vehicles, in biomedical imaging, as nanomaterials, etc. [52]. They can be generated in high quantities using diverse expression systems (bacterial, yeast, insect, and mammalian) depending on the desired properties. Bacteria and yeast are advantageous for their easy scale-up and low-cost, however, they are preferably utilized to produce VLPs containing one or two structural proteins without an envelope. On the other hand, the baculovirus/insect cells expression system provides a rapid and simple design procedure that is suitable for the production of vaccines against viruses whose structural proteins change between outbreaks. This system can perform complex post-translational modification (PTMs) compared to the bacterial/yeast systems, providing a high protein yield often greater than with mammalian cells and it is more affordable [5].

2.3 Decoration of VLPs

Due to their highly repetitive surface configuration, virus-like particles serve as a suitable antigen-presenting platform that can elicit a robust and long-lasting immune response even for the antigens with low immunogenicity [7]. In vaccine production, enhancement, and decoration of VLPs can be accomplished in various ways. The most widely used are chemical modifications and the genetic fusion of antigens with targeted viral proteins. Genetic fusion results in the simultaneous expression of the desired protein with the structural proteins that form VLPs. Even though this process can provide desirable results with smaller peptides/proteins, it can require a lot of time and resources for optimization. Additionally, it can lead to misfolding of components that impair their function and stability. One of the challenges is to find an adequate system for the expression and optimal production of VLPs and antigens due to the possible existence of distinct modifications [55]. Due to this, VLP and antigen are often expressed

separately and connected with chemical linkers. Binding via sulfhydryl groups (Cys) [56], attachment of Ni-NTA linkers to bind to His-Tag antigens [57], incorporation of unnatural amino acids for click conjugation [58], are some examples of methods that can be used to bind antigens to VLPs. However, their use may be restricted due to heterogeneous/incomplete coverage of VLPs, inability to display complex antigens, the formation of unwanted chemical bonds that disrupt stability, etc. [58,59].

These disadvantages were addressed through the development of new conjugation methods that utilize the spontaneous formation of amide bonds between split units of bacterial proteins [59]. The SpyCatcher/SpyTag conjugation system is the pioneer method created by Howarth´s lab, proven to be efficacious in the decoration of VLPs for vaccine development [55]. This method also served as a baseline for generating similar systems like SpyLigase and SnoopLigase which was utilized in this research project [60].

2.3.1 SpyCatcher/SpyTag system: principles

This system is made by splitting and engineering the immunoglobulin-like collagen adhesin domain (CnaB2) from the fibronectin-binding protein (FbaB) present in the Gram-positive bacteria *Streptococcus pyogenes*. As a result, two components are made: SpyCatcher (138 amino acids) and SpyTag peptide (13 amino acids). SpyCatcher contains reactive lysine (K) and catalytic glutamate (E), which allows the formation of a stable isopeptide bond with aspartate (D) on the SpyTag peptide. This reaction occurs rapidly within minutes, even in a diverse onset of conditions (high temperatures, different pH values, and buffers) [59]. Also, both units can be fused to the proteins at multiple positions (N-terminal, C-terminal, and internal sites). SpyCatcher-SpyTag system has been used for different purposes including vaccine development, decoration of hydrogels, protein cyclization and increasing the resistance, labelling of molecules for high-resolution microscopy, etc. [60]. The SpyCatcher-VLPs have been produced and utilized in vaccine development for the display of SpyTag-antigens. The immunization of the mice has confirmed the immunogenic properties and efficiency of this novel approach [10,55,61]. However, due to its bigger size, SpyCatcher is likely to be less tolerable and may be the problem for the end-use of the product [9], such as masking the antigens from the immune system cells or inhibiting the activity of its fusion partner in some cases. The development of antibodies against SpyCatcher-VLPs [55] and SpyCatcher:SpyTag [62] has been reported previously however, it is still uncertain if this can have a negative effect on the immune response against presented antigens.

2.3.2 SnoopLigase system

SnoopLigase system is a relatively new peptide-peptide ligation method, based on SpyCatcher and SpyLigase system [60] with modulations that provide a certain advantage over those two other systems. SnoopLigase is an enzyme that catalyses site-specific transamidation and forms an isopeptide bond between two peptide tags, SnoopTagJr and DogTag. The components of this system were developed by splitting the C-terminal domain of RrgA adhesin protein from *Streptococcus pneumoniae* into three-parts. After splitting, these units were optimised using computational prediction (molecular structure and stability, as well as sequence homology) and validated through biochemical assays. Catalytic glutamate (E) on SnoopLigase promotes the covalent bond formation linking the reactive lysine (K) on SnoopTagJr and asparagine (N) on DogTag together [8]. Importantly, because of the relatively strong affinity between the components, the binding of SnoopLigase to HaloLink or streptavidin resin enables solid-phase conjugate purification followed by the removal of SnoopLigase from the final product [63]. There are three different methods reported for the removal of SnoopLigase. One method includes the elution by gradually increasing imidazole concentration while the other one uses acidic glycine buffer. The third method is based on the elution using peptide competitor SnoopTagJr:DogTag that competes with formed conjugation complex for binding to SnoopLigase. Once the peptide competitor binds to SnoopLigase, the conjugation complex is released from SnoopLigase [8].

Even though this technique shows lower yield and tolerance in compared to SpyCatcher/SpyTag technology, it can successfully overcome the problem of protein domain staying in the end-product which is present with SpyCatcher method [9].

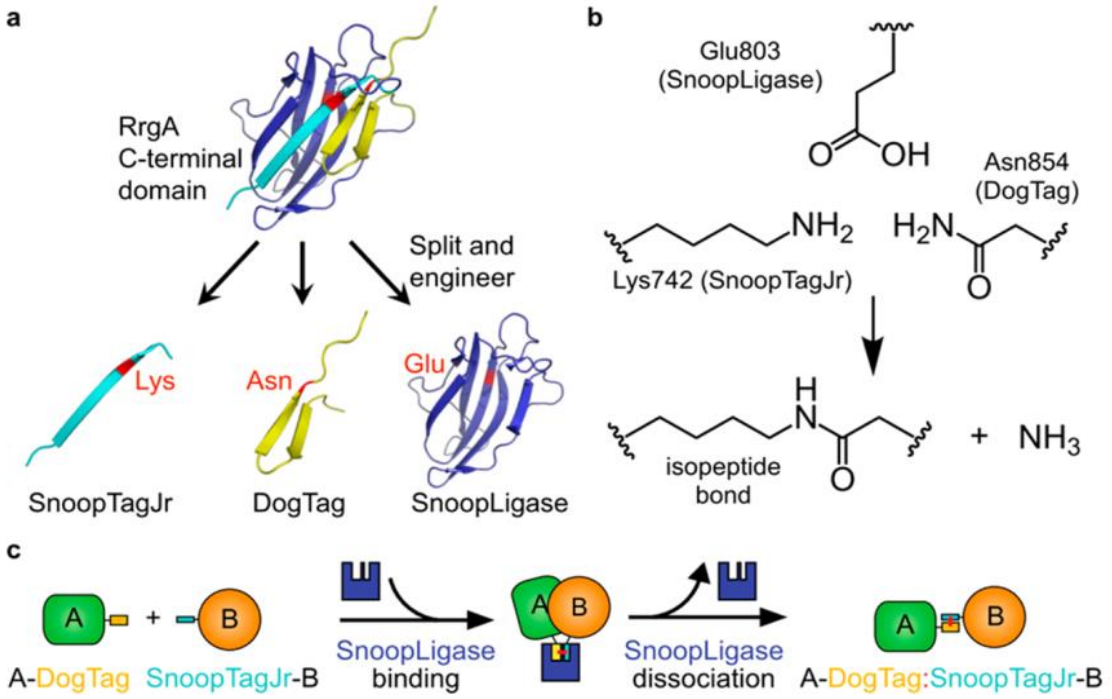

Figure 4. *Design of SnoopLigase system.* ***A)*** *The C-terminal domain of adhesin RrgA was split and engineered into three parts: SnoopTagJr (cyan), DogTag (yellow) and SnoopLigase (blue). The reactive residues are shown in red.* ***B)*** *Chemical principles of reaction: Glu803 (SnoopLigase) catalyses the formation of isopeptide bond between Lys742 (SnoopTagJr) and Asn854 (DogTag), generating ammonia.* ***C)*** *The principle of SnoopLigase system with linking DogTag and SnoopTagJr fused with proteins (A and B). After conjugation, SnoopLigase is dissociated from the end-product. Adapted from* [8].

SpyLigase is derived from the FbaB protein from *Streptococcus pyogenes* and utilizes a similar three-part system as SnoopLigase [64], except that SnoopLigase is made from a protein that shows better thermodynamic driving force. SnoopLigase shows a much higher yield and endurance to different types of conditions compared to SpyLigase since it tolerates a great variety of buffers and temperatures [8,60]. Also, SpyLigase reaction requires precise and inconvenient conditions that are important for folding stability, while SnoopLigase is modified into a more rigid form to make a better and stable catalyst that can function in different environments [8].

SnoopLigase system was also tested for vaccine development, where malaria and cancer antigens were fused to SnoopTagJr and successfully linked with the DogTag-IMX313 nanoparticle. The results reported showed the enhanced antibody response against two malarial antigens, and that including or removal of SnoopLigase from the conjugates did not have an impact on desired antibody response [9].

2.4 Vaccines and immunity:

2.4.1 Virus-like particles vaccines

Ever since their discovery in the 1960s, virus-like particles (VLPs) have been exceedingly utilized in vaccine research and development, due to their specific characteristic and adaptations. Mimicking the conformation and organization of native viruses, VLPs are used as immunogens in the production of prophylactic and therapeutic vaccines [52] . Due to the lack of a viral genome and infectivity, VLPs are very safe for production and usage. VLPs can be rapidly produced in large quantities using different expression systems [5], thus enabling the quick adaptation of VLP- based vaccines to the emergence of epidemic viruses. Their surface can be modified through genetic incorporation or chemical conjugation as described previously, allowing multivalent representation of homologous and heterogenic epitopes/antigens [52]. Until today, numerous VLP-based vaccines are approved for human application, such as Cervarix, Gardasil, and Gardasil-9 for human papillomavirus (HPV), Engerix-B, and Recombivax HB for hepatitis B virus (HBV), and Hecolin for hepatitis E virus (HEV). Multiple new VLP-based vaccines are currently in different phases of production and clinical trials [65].

Pathogen recognition receptors (PRRs) expressed on the surface of dendritic cells (DC) and endosomes can efficiently detect VLPs. The uptake and processing of VLPs in DC lead to the presentation of the peptide via the major histocompatibility complex (MHC) class I or class II, leading to the priming of cytotoxic ($CD8^+$) and helper ($CD4^+$) T cells [65,66]. The $CD4^+$ (Th2) cells can enhance antibody production stimulating B cells maturation and improving the cytotoxicity of $CD8^+$ (Th1) cells. Due to multimeric epitopes expressed on the surface of VLPs, cross-linking of B cell receptors (BCRs) is activated. This can induce T cell- independent activation of the B cell and antibody production. B cells can also function as antigen-presenting cells (APCs), taking VLPs and presenting antigens to T cells [67,68]. Therefore, vaccines based on VLPs can stimulate robust cell-mediated and humoral immune responses even without the assistance of adjuvants. However, most of the VLP-based vaccines use aluminum hydroxide (AH) to boost immunogenicity and strengthen the immune response [65].

Noroviruses are one of the major causes of acute gastroenteritis worldwide, causing symptoms such as diarrhea, vomiting, weakness, and headaches [69]. The viral capsid of ~40 nm is composed of 180 VP1 proteins arranged in 90 dimers. Recombinant expression of VP1 protein leads to the formation of VLPs that are structurally very similar

to a native virus [70]. Here in the Protein Dynamics research group, a VLP platform based on norovirus particles (genotype GII-4) has been well established during the past few years. The norovirus-like particles (noroVLPs) have been successfully produced and purified [78,79], genetically fused with His- tag (C-terminus) [57] and decorated with SpyCatcher/SpyTag system to make a modular vaccine platform [10]. The His-tag was utilized for purification and non-covalent conjugation that allowed the display of fluorescent dye molecule through Tris-NTA adaptors [57]. Later, the His-tag was substituted with the SpyTag for conjugation of noroVLPs with SpyCatcher-influenza antigens [72] and used for pre-clinical trials. The results showed the high antibody titers for conserved influenza antigen (HA2/H1F) and the high stability of the SpyTag-noroVLP platform, however, the antibodies against SpyCatcher were also present. There were no antibodies found against the M2e peptide [10], and the hypothesis is that SpyCatcher can potentially mask the antigens from the immune cells due to its size and immunogenicity. Therefore, in this study, we decided to test the SnoopLigase system for decoration of noroVLPs with SARS-CoV-2 antigens by replacing the SpyTag with DogTag in the construct. Due to the importance of spike glycoprotein in SARS-CoV-2 infection and high sequence conservation, we decided to utilize receptor-binding domain (RBD) and receptor binding motif (RBM) of spike glycoprotein as the most promising antigens for eliciting a strong immune response.

2.4.2 SARS-CoV-2 vaccines

The ongoing pandemic of the SARS-CoV-2 virus began in 2019 in China and spread quite quickly to all parts of the world. Until now, it has been estimated around 121 million infections, of which more than 2.67 million resulted in death outcomes. The consequences of the pandemic on human lives, health, and the economic situation are enormous, and therefore huge efforts are being made to alleviate and end current situation. Throughout history, it has been proven that the most effective measure of overcoming pandemic and epidemic pathogens is vaccination and the establishment of global herd immunity [73]. At the time of designing and beginning this thesis project, there was no approved vaccine against any strain of coronavirus. However, currently there are over 60 vaccines in various stages of clinical trials and several vaccines already approved for emergency usage. Developed vaccines are based on various technologies, including the use of inactivated viruses, viral-vectored vaccines, DNA and RNA vaccines, protein / peptide subunit vaccines, and live attenuated vaccines [74].

The first vaccine that was approved for early use in Russia is Sputnik V (Russian Federation) consisting of a recombinant adenovirus serotype vectors carrying the gene that encodes for spike glycoprotein. This vaccine was not authorized in most countries due to the lack of phase III trials data. In February 2021, the interim results of phase III trial were published in *The Lancet* indicating the efficiency of 91.6% achieved after second dose administration [75]. The documentation for marketing approval for global usage of this vaccine is still under examination.

The first two vaccines approved in EU and USA, BNT161b2 (Pfizer-BioNTech) [76] and mRNA-1273 (Moderna) [77] are messenger RNA vaccines (mRNA) that contain the genetic information for the production of SARS-CoV-2 spike glycoprotein. In both instances, the mRNA molecule is packed in a lipid nanoparticle to secure protection from degradation by natural enzymes in the organism. After injection, the lipid particles fuse with the cell releasing mRNA that serves as a template for the spike protein synthesis. The cell then displays the spike protein on the surface, which leads to the stimulation of the immune system that recognizes the protein as a foreign substance. While both vaccines require the injection of two doses (0.3 mL of vaccine solution per dose), the time between doses is different. The Pfizer-BioNTech vaccine is given for the second time 21 days after the first dose [76], while the time between doses of the Moderna vaccine is at least 28 days (0.5 mL of vaccine solution per dose) [77]. The biggest challenge of the Pfizer-BioNTech vaccine is the shipping and storage conditions since it requires special freezers (-75 °C) while the Modern vaccine can be stored at -20 °C. Another approved vaccine is ChAdOx1 (Oxford-AstraZeneca) [78] the contains the DNA sequence encoding the spike protein encapsulated in a chimpanzee adenovirus-vector. This vaccine works on the similar principle as the first two, with two doses required approximately 8-12 apart (0.5 mL of vaccine solution per dose). According to data from the phase I and phase II clinical trials, all three vaccines were able to induce the production of neutralizing antibodies against spike glycoproteins as well as the activation of the cell-mediated immune response. The efficiency of both mRNA-based vaccines has been reported to be more than 90%, while the DNA vaccine efficacy is around 70% [74]. The fourth vaccine that was recently approved for emergency use is Ad26.COV2.S (Johnson & Johnson) vaccine also containing DNA information for spike protein production packed into adenovirus-vector. Unlike other vaccines, this one is administered only as a single dose and can be stored at +4 °C [79].

The current results from phase III suggest that these vaccines provide protection from symptomatic SARS-CoV-2 infections. Clinical trials included tens of thousands of

participants of different age, ethnicity, and geographic location [74]. Both humoral and cellular immunity are needed to effectively fight viral infection and to achieve long-term immunity. It has been reported that the neutralizing antibodies naturally decline after infection over a span of a few months. Therefore, it was necessary to establish the existence of the specific T cells and memory immune cells. Recent studies provide a shred of strong evidence that the specific memory T and B cells are present for up to eight month post infection [80,81]. The interim data from all phases of clinical trials support the assumption that memory T cells and B cells response can offer sufficient and long-lasting immunity to SARS-CoV-2 [74].

However, many aspects of immunity and efficacy of the vaccines are still uncertain. There are several other vaccines approved only for certain countries and several vaccine candidates waiting for market authorization. Meanwhile, a few new SARS-CoV-2 variants emerged across the globe in the past few months. The most concerning are B.1.1.7 detected in the UK, B.1.351 variant from South Africa, and P.1 variant from Brazil. The mutations are mostly found in the spike glycoprotein which seems to increase the affinity towards receptor and elevate transmissibility [82]. Therefore, constant research and development are needed to adequately assess the potential obstacles and to prevent further fatalities. The establishment of a modular and fast-to-produce vaccine platform would be beneficial for situations like the current, where there is an urgent need for adequate and rapid response.

3. OBJECTIVES

The research aimed to produce and characterize norovirus-like particles decorated with coronavirus antigens. This research is part of a larger research project that aims to create a modular vaccine platform based on the norovirus-like particle. The platform should be able to respond to emerging pandemics, like the current coronavirus outbreak.

Specific aims of the study:

1. Production and purification of DogTag-noroVLPs, SnoopLigase, and SnoopTagJr-linked coronavirus antigens.
2. Decoration of the produced VLPs using the SnoopLigase system.
3. Removal of the SnoopLigase from the reacted complex.
4. Comparison of the DogTag/SnoopLigase conjugated particles with directly fused norovirus-coronavirus hybrids

Norovirus-like particles fused with His-tag were used for non-covalent binding of fluorescent dye molecule and streptavidin-biotin through Tris-NTA adaptors [57]. Later, His-tag was replaced with SpyTag, and utilization of SpyCatcher/SpyTag system allowed the generation of modular vaccine platform and decoration of noroVLPs with influenza antigens. This vaccine candidate was tested in pre-clinical trials and resulted in a potent immune response in mice [10]. However, there is a certain concern about the immunogenicity and size of SpyCatcher protein, which seems to be less tolerated [9] and can potentially mask the fusion partner from the immune system. To address this challenge, we decided to test the SnoopLigase system with noroVLPs, where SpyTag is substituted with DogTag and SnoopTagJr is fused with coronavirus (SARS- CoV-2) antigens. SnoopLigase is expected to catalyze formation on isopeptide bond between these two tags and afterward removed from the end-product. SnoopLigase system was already tested as a tool for decoration of nanoparticles and as a potential modular vaccine candidate [9].

4. MATERIALS AND METHODS

4.1 Main methods

4.1.1 SDS-PAGE and Western blot:

All proteins produced during this project were characterized and analysed by SDS-PAGE and Western blot. Initially, SDS-PAGE loading buffer containing reducing agent (β-mercaptoethanol) was mixed with samples and boiled at 100 °C for 10 minutes resulting in protein denaturation. Sodium dodecyl sulphate (SDS) binds to protein linear structure covering their intrinsic charge and introducing negative charge proportional to protein length. Afterwards, samples were loaded onto a polyacrylamide gel and proteins were segregated with electrophoresis according to their molecular weight. Three types of gel were used: self-made stain-free gel (TGX Stain-free Fast Cast, Acrylamide kit, 12%, #1610175), Any kD Mini PROTEAN TGX Stain-Free Protein Gel and Any kD Mini PROTEAN TGX Precast Protein Gels (Bio-Rad). Photoactivation and imaging of Stain-free gels was carried out with ChemiDoc XRS+ (Bio-Rad) using Stain-Free imaging technology (UV excitation). Trihalo compounds present in the gel matrix bind to tryptophan residues in proteins, increasing their fluorescence upon exposure to UV light, which allows protein detection for further quantification and analysis [83].

Detection of 5-FAM-SnoopRBM and its conjugates was done using Any kD Mini PROTEAN TGX Precast Protein Gel (Bio-Rad, #4569034) and Alexa Fluor 488 fluorescent blot imaging method with ChemiDoc XRS+ (Bio-Rad). 5-FAM (5-Carboxyfluorescein) is an amine-reactive fluorescent label used for *in situ* labelling of biomolecules. Its excitation peak is at 495 nm and emission peak at 520 nm [84].

For Western blot analysis, electroblotting of the gels onto nitrocellulose membrane was done with Trans-Blot Turbo Blotting System (Bio-Rad). For visualization of PageRuler Unstained Protein Ladders (Thermo Fisher Scientific, #26630), membranes were incubated in Ponceau S dye solution (Sigma-Aldrich) and marked by WesternSure Pen (LI-COR Biosciences, #926-91000). To inhibit unspecific antibody binding onto the membrane, blots were incubated in blocking buffer[1]. Following steps include incubation of membrane with primary and secondary antibody solutions, after each the membrane

[1] 5% bovine serum albumin (BSA)-tris-buffered saline (TBS) + 0.05% NaN_3

was washed three times with TBS-Tween 20 (5-10 minutes). Primary antibodies bind to specific target molecules, while secondary antibodies recognize and bind primary antibodies, which enhances signal amplification and visualization. The Tween 20 can potentially interfere with imaging signal, thus membrane was placed in TBS and imaged with Odyssey CLx system (LI-COR Biosciences).

Due to occasional malfunction of Odyssey CLx system, as an alternative method I used WesternBright ECL (Advansta, #K-12045-D20) Western blotting detection kit that requires Horseradish Peroxidase (HRP) conjugates as secondary antibodies. Following the final washing step, WesternBright ECL components were mixed 1:1 in adequate amounts needed to cover 0.1 ml/cm3 of membrane, placed on the blot and incubated for 2 minutes. After excess reagent was drained, blot was covered with plastic wrap and imaged with ChemiDoc XRS+ (Bio-Rad) using Chemi Hi Resolution method.

4.1.2 Chromatography methods:

Chromatographic purification of SnoopLigase, noroVLPs and coronavirus antigens was conducted with ÄKTA purifier 100 (GE Healthcare) instrument. Separation of proteins from impurities takes place in prepacked columns that were equilibrated with binding buffer before loading of sample. Unwanted material was washed away from the column and the target protein was eluted with elution buffer into fraction collector. Measurement of UV absorbance at 280 nm gave information about the elution time of proteins and their total concentration.

Immobilized metal affinity chromatography (IMAC) was used for purification of SnoopLigase and SnoopTagJr-RBD due to the presence of 6x-Histidine Tag on their N-terminus. IMAC is a specialized type of affinity chromatography where proteins are purified according to their affinity to specific metal ions ($Co^{2+,}$ Ni^{2+}, Cu^{2+}, Zn^{2+}) immobilized on a solid resin. The most common ion for purification of His-tagged proteins is Ni^{2+} because it exhibits high affinity and good selectivity for 6xHis-tagged proteins. The IMAC column contains Ni^{2+} ions embedded on sepharose/agarose beads via immobilized chelator group. In general, imidazole is used for elution of His-tagged proteins because it competes with the His-tag at binding to the resin, resembling the side chain of histidine [85].

DogTag-noroVLP samples were purified with sucrose-gradient centrifugation (described later in section 4.3.3) and then additionally with ion exchange chromatography (IEX) to

get rid of baculovirus DNA, RNA or intact virions. Ion exchange chromatography is based on adsorption and reversible binding of charged molecules to oppositely charged groups present on insoluble matrix. The pI value of a protein is used to determine buffer pH, which is crucial for protein binding and elution. If the protein is exposed to a pH lower than its pI, it will become positively charged and bind to cation exchanger and if the pH is above its pI, the protein will be negatively charged and bind to an anion exchanger [86].

4.1.3 Insect cells

Trichoplusia ni (Hi5) and *Spodoptera frugiperda* (Sf9) insect cells lines were utilized in this project for production of proteins/VLPs, baculovirus stock production (P1, P2 and P3) and determination of baculovirus titres. Cells were grown in Insect-XPRESS Protein-free insect cell medium with L-glutamine (Lonza Group AG) and maintained in two parallel 50 mL cultures (in case one gets contaminated) at +27 °C with shaking (~122 rpm). To avoid aggregation of Hi5 cells into clumps, 10 U/mL of heparin stock (Sigma-Aldrich) was added to the culture. Cells were monitored and passed three times a week during mid-log phase of growth. Production cell cultures were set by gradually increasing volume with appropriate cell concentration (early log-phase) and viability of > 90%. Counting of the cells and viability evaluation was performed with Countess Automated Cell Counter (Invitrogen).

4.1.4 Baculovirus stock productions

The baculovirus expression system was used to produce DogTag-noroVLPs and SnoopTagJr-RBD in insect cells. To generate recombinant baculovirus stocks, we utilized the *flash*BAC ULTRA system (Oxford Expression Technology, #100301) and pOET5 (Figure 5) transfection vectors containing gene of interest under polyhedrin promoter, manufactured, and shipped by GenScript.

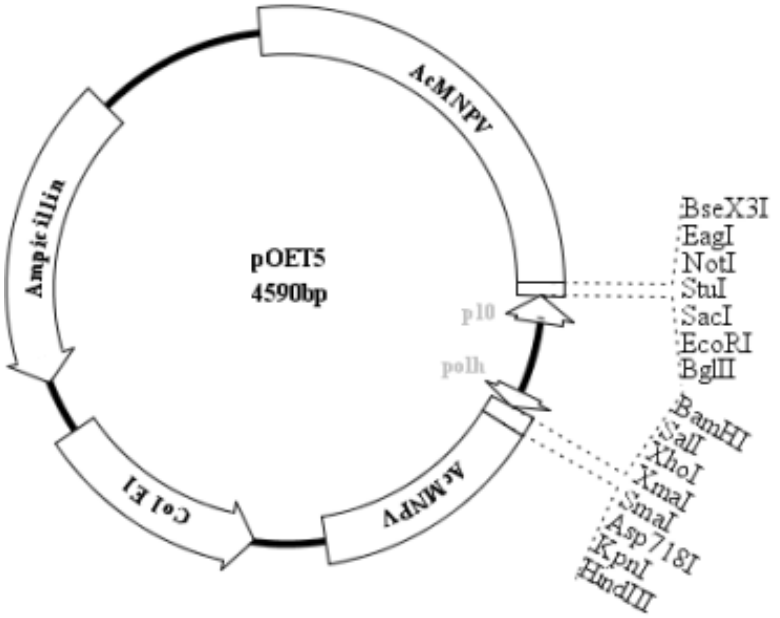

Figure 5: *pOET5 transfer vector is designed for simultaneous expression of two foreign genes and it is compatible for usage with flashBAC ULTRA system. It has two promoters: AcMNPV polyhedrin (polh) and p10 promoter placed in opposite orientation (to avoid recombination) and two multiple cloning sites (MSC). Ampicillin resistance gene and bacterial origin of replication allows amplification in E. coli. Adapted from* [87]

Recombinant baculoviruses were made according to BaculoFectin protocol [88]. Briefly, over 95% viable Sf9 cells in early log phase were transfected with the plasmid and BaculoFectin reagent. The recombinant baculoviruses were collected (P1 stock) after 6 days incubation with 1% fetal bovine serum (FBS) added to supernatant, before sterilizing through 0.2 µm filter and stored at +4 °C.

Sf9 cells (> 95% viable) with cells density of 2 x 10^6/mL (early log-phase) were used to produce higher baculovirus titres (P2 stock). P1 stock dilution 1:200 was used for 200 mL of cell culture after which suspension was incubated for 6 days at +27 °C with shaking (~122 rpm) inside MaxQ800 incubator. P2 stock was harvested by adding 1% FBS to production cultures and centrifugation (Eppendorf centrifuge 5810 R) at 1000 g for 5 minutes. Supernatant was collected, filtered subsequently through Nalgene Rapid-Flow 0.45 µm and 0.2 µm vacuum filters (Thermo Fisher Scientific) with Integra VACUSAFE (Integra Biosciences) and stored at +4 °C. Cell pellet was stored at -20 °C for recovering of more baculoviruses in future, if necessary.

Production of P3 baculovirus stocks included the same steps as in P2 stock production, except we used 600 mL cell culture volumes (2 x 300 mL) and Sartoclear Dynamics Lab Filter Aid (Sartorius AG, #150190419) to harvest baculovirus stocks. The 10 g of filter

aid and 1% FBS was added to the cell suspension, mixed properly, and filtered through Nalgene Rapid-Flow 0.2 µm vacuum filter to ensure sterile solution. The baculovirus P3 stock solution was stored at +4 °C for use in protein and noroVLP production.

4.1.5 Titration of recombinant baculovirus stocks

Determination of baculovirus stock (P3) titres was conducted with the BacPAK Baculovirus Rapid titre Kit immunoassay (Takara Bio, #631406) that detects viral envelope glycoprotein (gp64) and indicates the ability of virus to infect cells. The results of this assay are expressed as infectious units per ml (IFU/mL) which is an indicator of virus capability to infect a cell. This information is crucial for determination of optimal multiplicity of infection (MOI) that represents a ratio of infectious virions to the cells in suspension (no. of virions added/no. of cells). The whole process was carried out by following the exact protocol given by manufacturer [89].

4.2 SnoopLigase

4.2.1 Plasmid amplification and extraction

pET28a-AviTag-SnoopLigase plasmid (Figure 6) was constructed by the Mark Howarth Lab [8] and ordered from Addgene (Massachusetts, USA). The plasmid has an N-terminal AviTag for site-specific biotinylation and 6x-Histidine Tag for affinity chromatography purification.

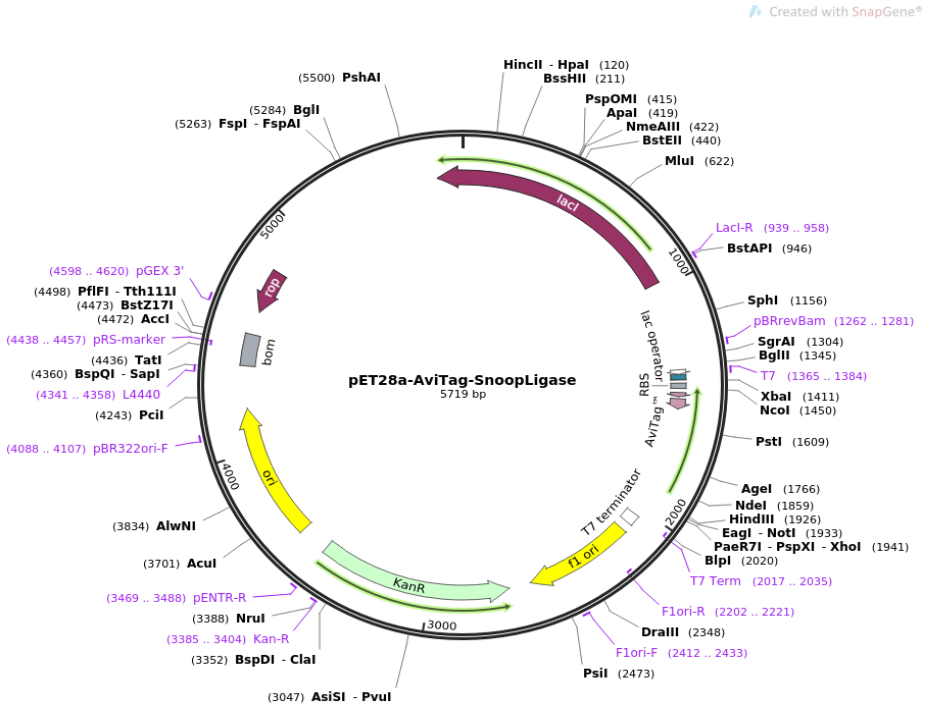

Figure 6: *pET28a-AviTag-SnoopLigase (Addgene plasmid ID 105626). Adapted from* [90]

The plasmid was delivered as transformed bacteria in stab culture format. A single colony was selected using a sterile loop and placed into Lysogeny broth (LB) medium containing kanamycin (50 µg/mL) and glucose (0.5% w/v). The bacterial cultures were grown at +37 °C for ~6 hours with constant shaking in the incubator (~200 rpm) until OD600 ~0.6. The cell suspension was then centrifuged in Sorvall LYNX 4000 (Thermo Fisher Scientific) for 10 minutes at 4000 rpm. The preparation of the large overnight (o/n) culture was done by diluting the starter culture 1:1000 into growth medium (LB-Kanamycin-glucose) and grown o/n at +37 °C with shaking ~200 rpm in the incubator. Endotoxin-free purification of plasmid was done with NucleoBond Xtra Midi Plus EF (Macherey-Nagel, #1908/001) according to the manual. Determination of plasmid yield was done with NanoDrop 2000/One spectrophotometer (Thermo Fisher Scientific). SnoopLigase plasmid was verified by sequencing of plasmid DNA and result from analysis using SnapGene software (GSL Biotech LLC).

4.2.2 SnoopLigase production:

SnoopLigase plasmid was transformed into *E. coli* BL21 (DE3) Star cell line using a heat shock transformation method (42 °C, 30 sec). After heat shock, the mixture was enriched with 250 µL of Super Optimal Broth (SOC) medium, incubated for 1 hour at +37 °C and then placed on prewarmed Lysogeny broth (LB) agar plate with 0.1% glucose (w/v) and kanamycin (50 µg/mL). A single fresh colony was inoculated from the agar plate into

1:100 LB with 50 µg/mL kanamycin and 0.8% glucose (w/v). Cultures were grown at +37 °C, 200 rpm until OD_{600} was ~0.5. Protein production was induced with 0.42 mM of Isopropyl β-d-1-thiogalactopyranoside (IPTG) (Thermo Fisher Scientific, #15529019) and grown at +30 °C, 200 rpm for 4 hours [8]. IPTG is allolactose analogue that binds to *lac* repressor and therefore enables the transcription of genes in *lac* operon. A few protein production cultures were incubated overnight at +25 °C to see if there is any difference in protein yield with slightly different incubation conditions. The production cultures were centrifuged at +4 °C, 4000 g for 10 minutes, pellets were collected and stored at -20 °C until purification. Glycerol stocks were prepared from several bacterial colonies, stored at -80 °C and used later for SnoopLigase production.

4.2.3 SnoopLigase purification and characterization

Cell pellets were resuspended in binding buffer[1] and cell lysis was achieved with Emulsiflex-C3 homogenizator (Avestin) after two rounds with pressure of 60-80 psi. Cell lysate was collected and centrifuged for 12 minutes, at +4 °C and 15 000 g. ÄKTA purifier 100 chromatography machine (GE Healthcare) was prepared and used for IMAC purification of SnoopLigase (section 4.2.3). Supernatant was loaded onto prepacked HisTrap FF crude 5 mL column (GE Healthcare, #17-5286-01) which was previously equilibrated with binding buffer (5x column volume) and flowthrough (FT) was collected into a clean bottle. After sample loading, the column was washed with binding buffer (5-10x column volume) and SnoopLigase was eluted into fractions (1.5 or 12 mL) using linear (20 to 500 mM over 20x column volume) or stepwise gradient (125, 350 to 500 mM) of imidazole present in elution buffer[2]. Elution fractions were chosen based on absorbance peak position (280 nm) and collected for SDS- PAGE and WB analysis. Additionally, pellet, load, FT, and wash samples (30 µL) were also included in analysis.

All samples were run onto stain-free gel, analysed and electroblotted on nitrocellulose membrane for WB (protocol in section 4.1.1). For detection of His-Tagged SnoopLigase, we used monoclonal Mouse Anti-HisTag antibody (Invitrogen, #MA1-21315) diluted 1:10 000 in 1% BSA in TBS-Tween + 0.05% NaN_3. IRDye 800CW-conjugated goat anti-mouse secondary antibody (LI-COR Biosciences, #926-32210) (diluted 1:20 000 in TBS-Tween) recognized and bound to primary antibody on membrane that was imaged with Odyssey CLx system (LI-COR Biosciences) system.

[1] 20 mM $NaPO_4$, 500 mM NaCl, **20 mM imidazole** pH 7.4
[2] 20 mM $NaPO_4$, 500 mM NaCl, **500 mM imidazole** pH 7.4

After results analysis, samples with SnoopLigase were pooled together and dialyzed with Slide-A-Lyser Dialysis Cassette – 3 500 MWCO (Thermo Fisher Scientific, #66333) into storage buffer[1]. Following dialysis, protein was concentrated until reaching the desired concentration (~1.5 mg/mL), using Vivaspin 20 centrifugal concentrator, 3 000 MWCO PES membrane (Sartorius, #VS2091). Concentration was measured with NanoDrop One/OneC Microvolume UV-Vis Spectrophotometer (Thermo Fisher Scientific) using predicted extinction coefficient and molecular weight information (ExPASy ProtParam). SnoopLigase was then aliquoted, flash-frozen in liquid nitrogen and stored at -80 °C. Later, concentration was remeasured with Pierce BCA Microplate Protein Assay Kit (Thermo Fisher Scientific, #23252) following the instructions in the manual [91].

4.2.4 Chemical biotinylation:

Chemical biotinylation was done using EZ-Link NHS-PEG12-Biotin reagent (Thermo Fisher Scientific, # A35389). The hydrophilic polyethylene glycol (PEG) spacer arm improves water solubility of biotinylated protein, exhibits less aggregation upon storage and can be used for spacing the biotin moiety from region important for enzymatic activity. N- Hydroxysuccinimide (NHS) esters are frequently used as biotinylation reagents and in certain conditions, NHS-biotin uses nucleophilic attack to react with primary amino groups (-NH2) which results into amide bond formation and NHS release. The target sites in proteins are amines located at the N-terminus of each polypeptide and in the side chain of lysine (Lys, K) residues. Determination of biotin concentration used for the labelling was done by following the protocol given in manual [92]. The amount of reagent used depends on the amount of labelling we aim for and concentration of the protein we want to label. Therefore, it is important to regulate molar ratio of reagent to target protein. In this project, 5- to 20-fold molar excess of EZ-Link NHS-PEG12-Biotin (Thermo Scientific) was tested in different tubes with the same amount/concentration of SnoopLigase (65 µM). After mixing all the components together, reactions were incubated on room temperature for 30 minutes. Dialysis against storage buffer[2] was used to eliminate unbound biotin. Aliquots were taken from each reaction tube, before and after dialysis, and analysed by SDS-PAGE and WB.

[1] 50 mM Tris borate pH 8.0 or 50 mM Sodium borate pH 10
[2] 50 mM Tris borate pH 8.0

4.2.5 Enzymatic biotinylation:

Enzymatic biotinylation was performed using *E. coli* biotin ligase (BirA) enzyme (https://www.addgene.org/20857/), according to the protocol described in previous paper [93]. Unlike chemical biotinylation, which is non-specific and can produce heterogeneous products with possibly impaired function, enzymatic biotinylation is highly specific, able to recognize and bind biotin to the 15 amino acid AviTag peptide. SnoopLigase has AviTag sequence GLNDIFEAQ**K**IEWHE on its N-terminus, which is easily recognized by BirA enzyme that binds biotin on lysine residue (**K**). The AviTag-SnoopLigase (65 μM) was biotinylated with 50 μM BirA in PBS, plus 5 mM MgCl2, 20 mM ATP and 6 mM of D-Biotin. Mixture was incubated for 1 hour at +30 °C with gentle mixing on a rocking platform. After 1-hour, same amount of biotin and BirA was added and incubation was continued for another hour. Samples were then dialyzed to remove excess biotin in storage buffer, flash-frozen in liquid nitrogen and stored at -80 °C. Small samples (30 μL) were taken before and after dialyses for SDS-PAGE evaluation. Detection of biotinylated SnoopLigase was done according to the protocol described in previous studies [72,94].

4.3 DogTag-norovirus-like particles

4.3.1 Plasmid preparation and amplification

DogTag-noroVLPs were produced using the baculovirus expression system and insect cells (as described in section 4.1.4). The gene encoding for DogTag-noroVLPs was subcloned into pOET5 plasmid (Figure 1) and placed downstream of the polyhedrin promoter, between BamHI and HindIII restriction sites. VP1 and DogTag sequence were separated with SpeI restriction site and GG linker *(Sequence in Appendix*). Plasmids were synthetized by GenScript (New Yersey, USA) and delivered in lyophilized form (100 ng/mL). Prior to amplification, the plasmids were dissolved in Tris-EDTA (TE) buffer[1] and transformed into *E. coli* TOP10 cells by heat shock method. Cell culture growth and plasmid extraction were done the same way as with SnoopLigase. The only exception was growth medium composition (LB-ampicillin-glucose) since pOET5 plasmid carries gene for ampicillin resistance.

[1] 10 mM Tris-HCl, 1 mM disodium EDTA pH 8

4.3.2 DogTag-noroVLP production

Production of DogTag-noroVLPs was done in Hi5 insect cell cultures (density 2 x10^6/mL) that were in early-log phase (viability > 95%). Heparin stock was added into final concentration of 10 U/mL to prevent cell aggregation. P3 baculovirus stock was used to infect cells at different MOI values: 0.5, 1, 1.5 and 2. Each production culture had the same volume (200 mL) in order to compare which MOI value results in highest production yield. Infected cell cultures were incubated at +27 °C with shaking (~122 rpm) and product was collected 6 dpi (days post infection) using Sartoclear Dynamics Lab Filter Aid (Sartorius AG) and Nalgene Rapid flow 0.2 µm vacuum filters. Starting material sample (1 mL) was taken for later SDS-PAGE and Western blot analysis.

4.3.3 Purification using sucrose density gradient centrifugation

Density gradient centrifugation utilizes sucrose gradient and high-speed ultracentrifugation to separate particles in solution based on their density. Sucrose cushion is made by adding 6 mL of 30% sucrose[1] into 38 mL Ultra-Clear centrifuge tubes (Beckman Coulter, #C14292). Clarified noroVLP supernatant (31 mL) was poured slowly on top of the sucrose cushion in each tube. Centrifugation was set at speed of 32 000 rpm (175 000 g) at +4 °C, for ~16 hour in Optima XE-100 ultracentrifuge and swinging-bucket rotor SW32Ti (Beckman Coulter). Thereafter, supernatant was discarded into endotoxin-free bottle, small sample was taken, and rest of the droplets were dried with cellulose paper. Endotoxin-free PBS (1.5 mL/tube) and magnetic stirring rods were used to dissolve pellets during a 4-hour (or o/n) incubation at +4 °C (in cold room). Following steps required solution resuspension and centrifugation with 13 000 g in Eppendorf 5424 R microcentrifuge for 5 minutes at +4 °C. Supernatant was collected without touching the pellet, filtered with Whatman Puradisc 25 AS Disposable Filter Device 0.2 µm (GE Healthcare) using syringe and stored at +4 °C. Small pellet sample was taken for further analysis.

4.3.4 Ion Exchange Chromatography

Following density gradient centrifugation, in order to accomplish higher level of purity, some samples were additionally purified using IEX with ÄKTA purifier 100 (GE Healthcare) as described previously (section 4.1.2). Initially, samples were resuspended in dilution buffer[2] in a ratio that lowers conductivity to < 3 mS/cm. VLP solution was

[1] 30 g sucrose in 100 mL PBS; sterilized and stored at +4 °C
[2] 20 mM phosphate buffer pH 7.0

loaded on a pre-packed anion exchanger HiTrap Q XL 5 mL column (GE Healthcare, #17515901) with a flow rate of 1 mL/min and flow-through was collected into clean bottle. Proteins that were bound weakly to the resin were washed off with binding buffer[1] (wash collected), while noroVLPs were eluted by gradually increasing salt concentration in elution buffer[2]. Eluted samples were fractionated into 5 mL samples and their analysis was based on A280 and A260 absorbance curves. Identification of noroVLPs was done with SDS-PAGE and Western blot according to the protocol explained earlier in section 4.1.1. Mouse anti-SpyTag-noroVLP antibody (MP23) (in-house polyclonal) [10] (diluted 1:1000 in 1% BSA-T + 0.05% NaN_3) solution was utilized for detection of noroVLPs and secondary IRDye 800CW goat anti-mouse (LI-COR Biosciences, #926-32210) (diluted 1:20 000 in TBS-T) was used for visualization by Odyssey CLx system.

Based on the result, samples were pooled together, dialyzed against PBS, and concentrated with Vivaspin 15 centrifugal concentrator, 10 000 MWCO PES membrane (Sartorius AG, #VS15T02). VLPs were stored at +4 °C and concentration was measured with Pierce BCA Microplate Protein Assay Kit [91] (Thermo Fisher Scientific, #23252).

4.3.5 Size, homogeneity, and stability measurements

Evaluation of noroVLPs size and homogeneity in solution was done with dynamic light scattering (DLS) using Zetasizer Nano ZS (Malvern Instruments). DLS measures Brownian motion of particles in solution to determine their hydrodynamic size. The results are based on three measurements (each consisting of 15 readings, 15 seconds each) at +25 °C.

The thermal stability of DogTag-noroVLPs was determined with Differential scanning fluorometry (DSF) using a CFX96 Touch Real-Time PCR Detection System (Bio-Rad). This system utilizes a qPCR instrument to monitor protein denaturation induced by increase in temperature. It measures the increase of SYPRO Orange (Thermo Fisher Scientific) dye fluorescence that binds to hydrophobic regions of unfolded proteins [95]. Samples placed in a 96-well plate (Bio-Rad) were heated from +25 °C to 110 °C with fluorescence reads taken at 1 °C intervals every 30 seconds. Samples with known melting temperature (Tm) (SpyTag-noroVLP and native noroVLPs [10]) were also included in measurements to ensure results reliability and for comparison.

[1] 50 mM phosphate buffer pH 7.0
[2] 50 mM phosphate buffer, 1 M NaCl pH 7.0

4.4 Coronavirus antigens fused with SnoopTagJr

4.4.1 Construct design

For decoration of DogTag-noroVLPs we utilized two different coronavirus (SARS-CoV-2) antigens fused with SnoopTagJr: SnoopTagJr-RBD (Receptor-binding domain) and SnoopTagJr-RBM (Receptor-binding motif).

SnoopTagJr-RBM is a 30-amino-acid peptide (SARS-CoV-2 Spike glycoprotein aa sequence 487-515), chemically synthesized and delivered in lyophilized form by a commercial provider (GenScript). This construct contains three experimentally confirmed T cell epitopes that are uniform between SARS-CoV and SARS-CoV-2 [96]. To enable identification of the conjugated complex, we ordered a version of SnoopTagJr-RBM labelled with 5FAM (5(6)-carboxyfluorescein) on its N-terminus. Both constructs (purity > 94%) were validated with mass spectrometry by the vendor (*Sequence in Appendix*).

SnoopTagJr-RBDs were produced in insect cells, using the baculovirus expression system (section 4.1.4), similarly as DogTag-noroVLPs. Genetic construct included a honeybee melittin signal peptide for efficient secretion in insect cells [97], 6x-Histidine Tag for affinity chromatography purification, TEV site, linker and SnoopTagJr at C-terminus to avoid possible clash with noroVLP upon conjugation. This construct was subcloned into pOET5 plasmid, between XhoI and KpnI restriction sites. *(Sequence in Appendix)*

4.4.2 SnoopTagJr-RBD production

Hi5 cells (viable > 95%) in concentration of 2 x10^6/mL were used for protein production after cell infection with different MOI values (0.5, 1, 1.5, 2 and 2.5) of P3 baculovirus stock. Infected cell suspensions (200 mL) were incubated for 6 days at +27 °C in incubator with constant shaking (122 rpm). Afterwards, product was collected with Sartoclear Dynamics Lab Filter Aid (Sartorius AG) and Nalgene Rapid flow 0.2 µm vacuum filters (Thermo Fisher Scientific). Small sample (1 mL) of each production was taken for further analysis and comparison.

4.4.3 SnoopTagJr-RBD purification

Due to the 6xHistidine Tag present on N-terminus of SnoopTagJr-RBD, purification was conducted in the same way as reported for SnoopLigase (section 4.4.3) with a slight change in binding[1] and elution buffer[2] composition. Prior to purification, samples were centrifuged for 30 minutes (+4 °C) at 20 000 rpm to remove aggregates. Supernatant was collected and loaded on HisTrap excel column (5 mL) (GE Healthcare, #17371206). Based on the absorbance results, elution fractions were analysed on SDS-PAGE and WB together with Load, FT, and Wash samples. Mouse Anti-HisTag antibody (Invitrogen, #MA1-21315) (diluted 1:10 000 in 1% BSA in TBS-Tween + 0.05% NaN3) was used to detect Histidine tag and IRDye 800CW-conjugated goat anti-mouse antibody (LI-COR Biosciences, #926-32210) (diluted 1:20 000 in TBS-Tween) for visualization by Odyssey CLx system. As an alternative, HRP Anti-mouse IgG (H+L) secondary antibody (Vector Laboratories, # PI-2000-1) (diluted 1:12 000 in TBS-Tween) solution was utilized with WesternBright ECL kit (Advansta, #K-12045-D20) to image a WB membrane with ChemiDoc XRS+ (Bio-Rad, Hercules, California, USA).

Highest quality samples were pooled together, dialyzed in PBS, and concentrated with Vivaspin 15 centrifugal concentrator, 10 000 MWCO PES membrane (Sartorius AG). Protein solutions were aliquoted, flash-frozen in liquid nitrogen and stored at -80 °C.

4.5 Conjugation reactions

To test the ability and efficiency of SnoopLigase to catalyse conjugation reaction and decorate DogTag-noroVLPs with SnoopTagJr-antigens, the products were mixed in the recommended buffer[3] [63] and incubated for 24/48 hours at +4 °C or RT. The usual reaction mix setting included DogTag-noroVLPs in a standard concentration (5 μM) and SnoopTagJr-antigens/SnoopLigase in 2-fold molar excess. We separately evaluated the effect of 15% glycerol (v/v) on conjugation rate, PBS as a reaction buffer, different molar excess of SnoopTagJr-antigens/SnoopLigase and efficacy of differently biotinylated SnoopLigase to form a conjugation complex. In the conjugation experiments we also included the control reactions, which included DogTag-MBP and SnoopTagJr-MBP proteins, given to us by Howarth´s lab (University of Oxford). We tested the conjugation

[1] 20 mM NaPO4, 500 mM NaCl, 20 mM imidazole pH 7.2
[2] 50 mM NaPO4, 500 mM NaCl, 500 mM imidazole pH 7.3
[3] 50 mM Tris borate, pH 7.5 + 15% glycerol (v/v) [63]

of SnoopTagJr-MBP with DogTag-noroVLPs and DogTag-MBP using (biotinylated) SnoopLigase produced in our lab.

The morphology analysis of conjugated DogTag-noroVLP was conducted with Jeol F200 S/TEM transmission electron microscope (TEM) (Jeol Ltd.) after samples were treated with 1% uranyl acetate (negative staining).

4.5.1 Evaluation of conjugation rate

The conjugation reactions were stopped with 5X SDS loading buffer (with β-mercaptoethanol), boiled at 100 °C for 10 minutes and analysed in SDS-PAGE. The gel was imaged with ChemiDoc XRS+ using either Stain-free method or Alexa 488 (section 4.1.1). Western blotting was used to confirm conjugation success by detecting His-tag on SnoopTagJr-RBD. The intensity of protein bands (densitometry) on gel were quantified with ImageLab software (Bio-Rad) and conjugation efficiency rate was calculated based on comparison between proportion of unconjugated DogTag-noroVLP with % of conjugated particles in one well (% of unconjugated + % of conjugated = 100%). For example, if there are 30% of conjugated particle out of 100% of particles in total (where 70% are unconjugated), then conjugation rate is estimated to be 30%.

4.5.2 Removal of SnoopLigase

The experiment was based on conjugation reactions with biotinylated (BirA) SnoopLigase and utilization of streptavidin resin in combination with gradual increase of imidazole concentration in order to separate Biotin-SnoopLigase from end product. The protocol mostly followed and combined the instructions given in several other papers [8,9,63] with minor changes in imidazole concentration. Based on unpublished measurements conducted earlier in Protein Dynamics group, imidazole concentration of 2.5 M can induce changes in noroVLP size and polydispersity index (PdI) which can possibly be reversed by dialyzing particle into PBS.

DogTag-noroVLP at 5 μM was incubated with 2-fold molar excess of SnoopLigase and SnoopTagJr-RBD in reaction buffer[1] for 48 hours at +4 °C. First, the streptavidin resin was washed and equilibrated with reaction buffer five times, each followed by centrifugation at 300 g for 30 sec. Conjugation reactions were then incubated with streptavidin resin and mixed by inverting for 1 hour on RT. The resin was then placed in Pierce Spin column (Thermo Fisher Scientific) and centrifuged (Eppendorf 5424 R) for

[1] 50 Mm Tris borate pH 7.5 + 15% glycerol (v/v)

30 sec. at 100 g and the wash sample was collected. Next step includes the resin wash (5x) with Tris-phosphate pH 7.0 [1], with 1 M imidazole pH 7.0 and 0.01% (v/v) Tween 20 on RT. For removal of residual liquid, resin was centrifuged again on 100 g for 30 sec. To elute the conjugates, resin was incubated with Tris phosphate with 2.5 M imidazole (both pH 7.0) for 5 minutes on RT with slow vibrations followed by centrifugation. This step was repeated twice to ensure removal of any remaining Biotin-SnoopLigase. The elution products were then dialysed in PBS using the Vivaspin 500, 10 000 MWCO PES (Sartorius AG, # VS0102) and stored at -80 °C. In each step of the process, samples were collected for SDS-PAGE analysis.

[1] 25 mM phosphoric acid adjusted to pH 7.0 with Tris base

5. RESULTS

5.1 SnoopLigase

5.1.1 Production, purification, and characterization of SnoopLigase

Production of SnoopLigase was accomplished in *E. coli* BL21 (DE3) Star cell line using LB-kanamycin-glucose growth medium. To test different growth conditions, a few production cultures were incubated for four hours, while some were left for overnight incubation. The four-hour cultures and overnight cultures were purified separately, compared with SDS-PAGE analysis and concentration measurement.

The 6x-Histidine tag was utilized for IMAC purification of SnoopLigase (section 4.2.3). For the first purification trial, we loaded a crude sample of 200 mL SnoopLigase production culture in order to test whether we are going to obtain efficient purification with high purity protein samples. The elution of SnoopLigase was induced with linear gradient increase of imidazole and eluted samples go through UV detector and then fraction collector. Based on the 280 nm absorbance curve, protein samples were collected and analysed with SDS-PAGE and Western blot. For detection of SnoopLigase in WB after first IMAC purification, we utilized mouse Anti-HisTag antibody (Invitrogen) and as a positive control (+), we used HisTag-control protein (hTalH1, MW~48kDa) produced in our research lab [98] (Figure 7A). The protein band in SDS-PAGE and WB matches with the theoretical molecular weight of SnoopLigase (~15.4 kDa). Information obtained from the first purification data analysis (data not presented) showed that the SnoopLigase gets eluted during a second higher elution peak, and therefore we made a method utilizing a stepwise increase of imidazole to collect fractions with a high concentration of protein.

During the first increase of imidazole concentration (first small peak), most of the impurities got eluted, while during the second increase (high peak) we got a high concentration of SnoopLigase eluted (Figure 7B). The chromatogram for both overnight and four-hour production cultures looked almost identical since we used the same method. However, according to the protein band intensity (Figure 7C), four-hour production cultures showed a higher protein concentration.

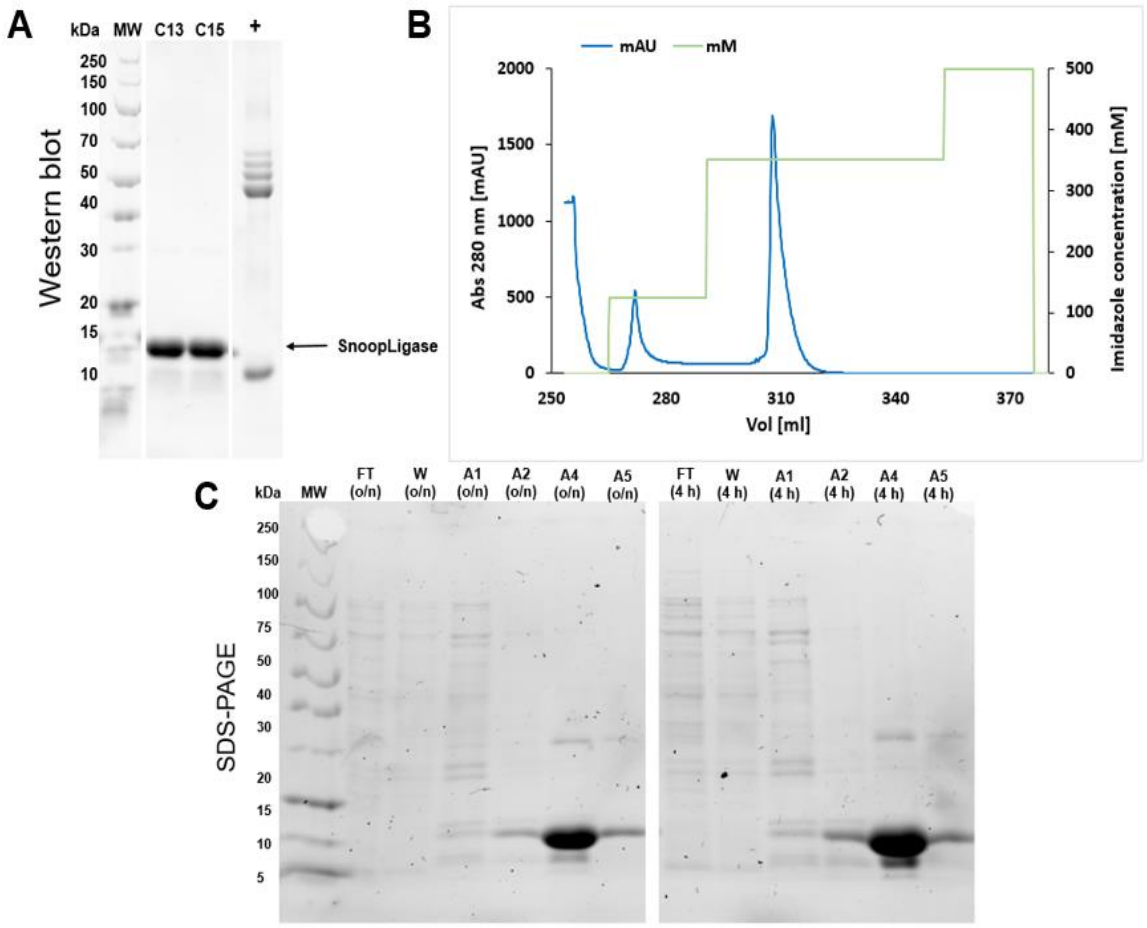

Figure 7. *Purification and characterization of SnoopLigase.* ***A)*** *Western blot membrane was treated with Anti-HisTag antibodies to detect SnoopLigase which is indicated with an arrow. HisTag-control protein (hTalH1) represent positive control shown as "+" and appears to have undergo some proteolytic processing. The image was taken with the Odyssey CLx system.* ***B)*** *IMAC chromatogram after introducing stepwise imidazole gradient elution (125, 350 to 500 mM). The protein absorbance (280 nm) curve is illustrated as a blue line.* ***C)*** *SDS-PAGE analysis of Stain-free gel with samples (4 µL/well) obtained after stepwise IMAC purification of overnight (o/n) and four-hour (4 h) production cultures. Flowthrough (FT) and wash (W) samples are also included. The image was taken with ChemiDoc XRS+.*

This was confirmed with total protein concentration measurements using NanoDrop, where overnight production resulted in 1.592 mg/mL of SnoopLigase, while four-hour production showed a concentration of 2.465 mg/mL. The total sample volume was the same is both purification end products. Thereafter, all the samples were pooled together, dialysed in storage buffer, concentrated, and stored at -80 °C. The total production yield was estimated to be around 20 mg/L with a purity of ~90% combining all purified samples.

5.1.2 Biotinylation of SnoopLigase

Biotinylation of SnoopLigase was tested using two different approaches. One experiment included chemical biotinylation with NHS-PEG12-Biotin reagent in which a biotin molecule gets attached to one or more lysine residues present in a molecule. This process included the mixture of SnoopLigase in fixed concentration with a 5- to 20-fold molar excess of NHS-PEG12-Biotin reagent (described in 4.2.4). The tubes were incubated on RT for 30 minutes, allowing the chemical reaction to occur. Chemical biotinylation of SnoopLigase has not yet been reported in any previous scientific research papers, therefore we wanted to test if the chemical biotinylation will have any effect on enzyme catalytic activity. The second biotinylation experiment was based on the utilization of biotin ligase (BirA) enzyme which recognizes and binds one biotin molecule specifically to AviTag positioned on the N-terminus. BirA biotinylation of SnoopLigase was already reported in [8,9,71] and the whole process was described in section 4.2.5.

The success of biotinylation was determined with SDS-PAGE and Western blot (Figure 8). For WB analysis, samples were previously incubated with engineered version of chicken avidin (CNCA) [99] that binds to biotin and enables recognition with polyclonal rabbit anti-avidin antibody (University of Oulu, Finland).

The SDS-PAGE results of chemical biotinylation (Figure 8A) for each fold reaction resulted in a differently biotinylated SnoopLigase molecule. The molecular weight of NHS-PEG_{12}-Biotin is ~941 Da and upon binding of one or more PEG_{12}-biotin molecule on lysine residues, the protein band shifts upwards. SnoopLigase contains ten lysine amino acids in total, which can explain the protein band shift in the gel up until 25 kDa (e.g. 10xbiotin of 941 Da + 15.4 kDa of SnoopLigase).

Enzymatic biotinylation was harder to detect only by SDS-PAGE, since a single biotin molecule binds to SnoopLigase, hence there was no distinguishable protein band shift seen in the gel (data not shown). Instead, Western blot data indicated the presence of Biotin-SnoopLigase (Figure 8B). As a positive control, we used both biotinylated BSA bound to CNCA and CNCA alone. Unbiotinylated SnoopLigase (alone or with CNCA) served as a negative control. According to the comparison of protein band intensity from SDS-PAGE and WB, it seems that most of the SnoopLigase get biotinylated.

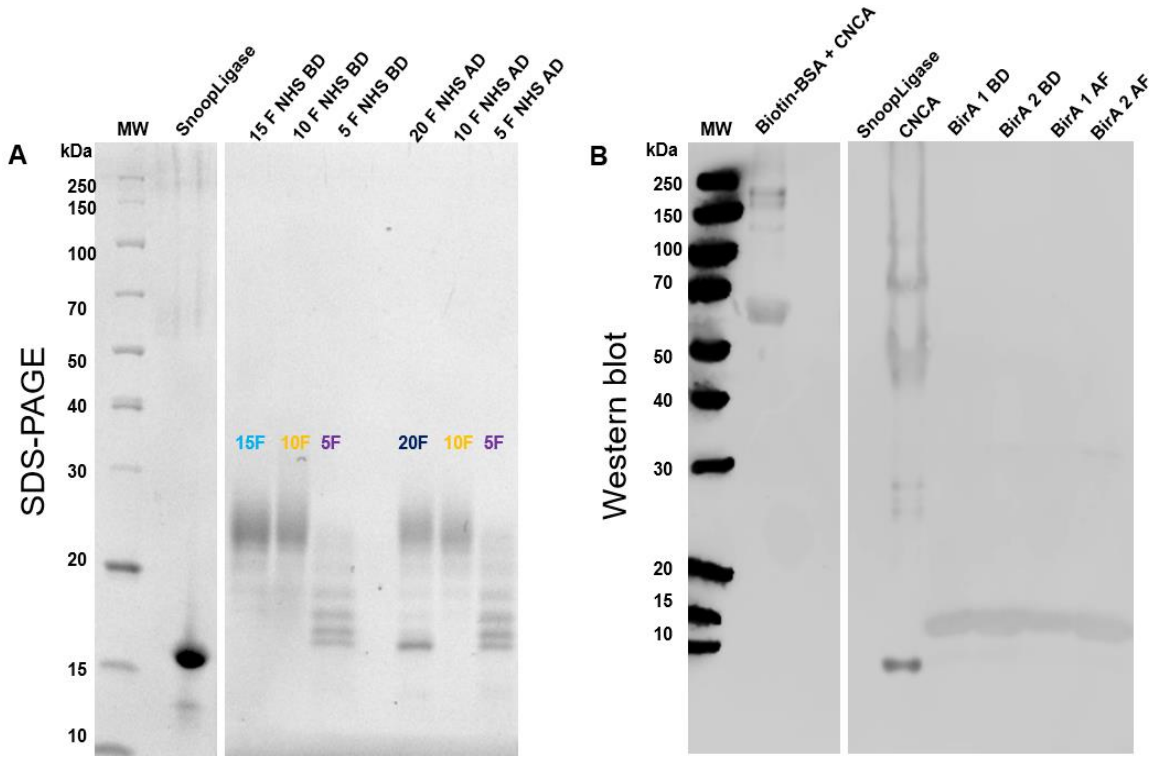

Figure 8. *Biotinylation of SnoopLigase.* ***A)*** *SDS-PAGE results of chemical biotinylation with a different molar excess of NHS-PEG$_{12}$-Biotin are also illustrated with certain colours. All samples were loaded (5 µL/well) onto Stain-free protein gel and imaged with ChemiDoc XRS+. The "F" stands for molar fold excess, "BD" for samples taken before dialysis and "AD" after dialysis.* ***B)*** *Western blot data shows the results after enzymatic biotinylation (BirA). Biotin-SnoopLigase was detected with anti-avidin antibodies as well as the positive controls. The image was obtained with the* Odyssey *CLx system.*

5.2 Titration of recombinant baculovirus stocks

The baculovirus stocks required for producing DogTag-noroVLPs and SnoopTagJr-RBD were made in Sf9 insect cell line following the same protocol (section 4.1.5). The P3 stock of SnoopTagJr-RBD was produced twice, due to a relatively low titre and demand for additional protein production. Infectivity of baculovirus stocks was determined with BacPAK Baculovirus Rapid Titre Kit (Takara Bio). This assay is based on immunostaining of infected cells by antibody detection of the viral envelope glycoprotein (gp64) which further reveals information about viral infectivity. The results are used to determine an MOI value needed for optimal protein production. Sf9 cells were used for infection with three different viral dilutions (10^{-4}, 10^{-5} and 10^{-6}). Positive and negative controls were also included in the assay as indicators of reliable results. HRP conjugate antibody was used for recognition of mouse gp64 antibody, which allowed clear visualization of infected foci under a light microscope after incubation in Blue Peroxidase Substrate. Virus titres were calculated based on the number of average foci for each dilution, which also defines the MOI value (Table 1).

	Virus dilutions			
Virus stock	**10^{-4}**	**10^{-5}**	**10^{-6}**	**Virus titer (IFU/mL)**
DogTag-noroVLP	$1.80*10^7$	$9.33*10^6$	ND	$1.37*10^7$
SnoopTagJr-RBD	$1.72*10^7$	$2.67*10^7$	$5.33*10^7$	$2.19*10^7$
SnoopTagJr-RBD 2nd	$2.07*10^7$	$2.07*10^7$	$1.33*10^7$	$2.23*10^7$

Table 1. *Baculovirus stock titres of DogTag-noroVLP and SnoopTagJr-RBD. The table represents the results of P3 stock titres in three different dilutions obtained with BacPAK Baculovirus Rapid Titre Kit, from which virus titres (IFU/mL) were calculated. There were no foci detected in 10^{-6} dilution of DogTag-noroVLP (marked as "ND").*

5.3 DogTag-norovirus-like particles

5.3.1 DogTag-noroVLP production

DogTag-noroVLP production was done in the Hi5 insect cell line, utilizing the recombinant baculovirus stocks made earlier. Previously, it has been demonstrated that noroVLP expression in Hi5 cells provides a much higher yield in comparison with Sf9 cells [72]. Also, it has been shown that MOI values of 1 and 0.5 seem to be optimal for noroVLP production [10,72]. Hi5 cells were infected with MOI: 0.5; 1; 1.5; 2 PFU/mL and incubated for six days in 200 mL culture volume. Production cultures were then collected, and a small start sample (SS) was taken from each production to conduct SDS-PAGE (Figure 9A) and Western blot (Figure 9B) characterization. The theoretical molecular weight of DogTag-noroVLP (~62 kDa) and isoelectric point (pI) were estimated based on the amino acid sequence using the ProtParam tool (https://web.expasy.org/protparam/; 27.5.2020). For Western blot detection, we utilized antibodies against SpyTag-noroVLP obtained previously from mouse sera (in-house product) [10]. We presumed that the DogTag-noroVLP can be recognized by these antibodies, since the noroVLP construct is the same for both, and SpyTag/DogTag despite being different, represents only a small portion of the particle. There was no significant difference between MOI values: 0.5-2 in production. Therefore, the finest MOI values were resolved to be 0.5 and 1 due to a similar yield and fewer impurities present.

Western blot data confirmed the presence of DogTag-noroVLP as well as a positive control (SpyTag-noroVLP). Negative control (SARS-CoV-2-VLP) was not detected, which can validate results credibility.

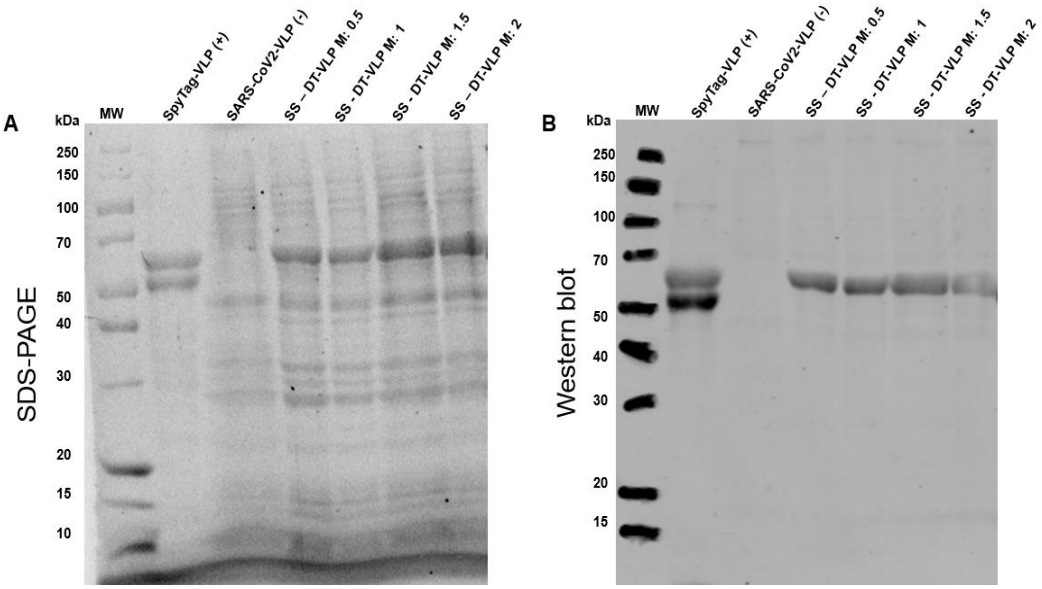

Figure 9. *Characterization of DogTag-noroVLPs start samples produced with different MOI values.* ***A)*** *SDS-PAGE results indicated the presence of DogTag-noroVLP at ~62 kDa, as expected. Start samples of DogTag-noroVLPs indicated as ´´SS-DT-VLP´´ were loaded onto Stain-free gel (5 µL/well) and imaged with ChemiDoc XRS+. MOI value is marked as ´´M´´.* ***B)*** *Western blot detection of DogTag-noroVLP was done with SpyTag-noroVLP antibodies (in-house product). SpyTag-noroVLP sample served as a positive control (+) and SARS-CoV-2-VLP as a negative control (-).*

5.3.2 Purification of DogTag-noroVLPs

DogTag-noroVLP samples were first purified by sucrose gradient ultracentrifugation. Sucrose cushion was placed at the bottom of centrifuge tubes, with noroVLP supernatant carefully placed on top of that. Overnight high-speed centrifugation allowed the separation of noroVLPs from other proteins/impurities based on their density (details in 4.3.3). All samples taken throughout this process were analysed on SDS-PAGE together with elution fraction samples from IEX (Figure 10B). To reach a higher degree of purity and get rid of baculovirus DNA, VLPs were additionally purified with Ion Exchange Chromatography (section 4.3.4). We utilized an anion exchanger column, from which noroVLPs were eluted by linear increasing of the salt gradient. Wash sample represents the first small peak on chromatogram (Figure 10A), and according to the SDS-PAGE results, a certain amount of noroVLP gets eluted during this step (Figure 10B). The noroVLPs elution lasts from 0.3 M until 0.5 M of NaCl concentration. Most of it gets eluted with 0.4 M, which is visible as the highest peak on the chromatogram (Figure 10A). Some other impurities got eluted with VLPs during this phase as well (fractions A2, A3 and A4). Load sample from this purification, as well as others (data not presented), shows that the noroVLPs samples were already quite pure after sucrose gradient centrifugation even though the protein band seems weak in this gel, possibly due to pipetting error. The purity

of DogTag-noroVLPs was estimated to be between 80-95%, depending on the different production cultures with a yield of ~16 mg/L. All samples were kept on +4 ºC.

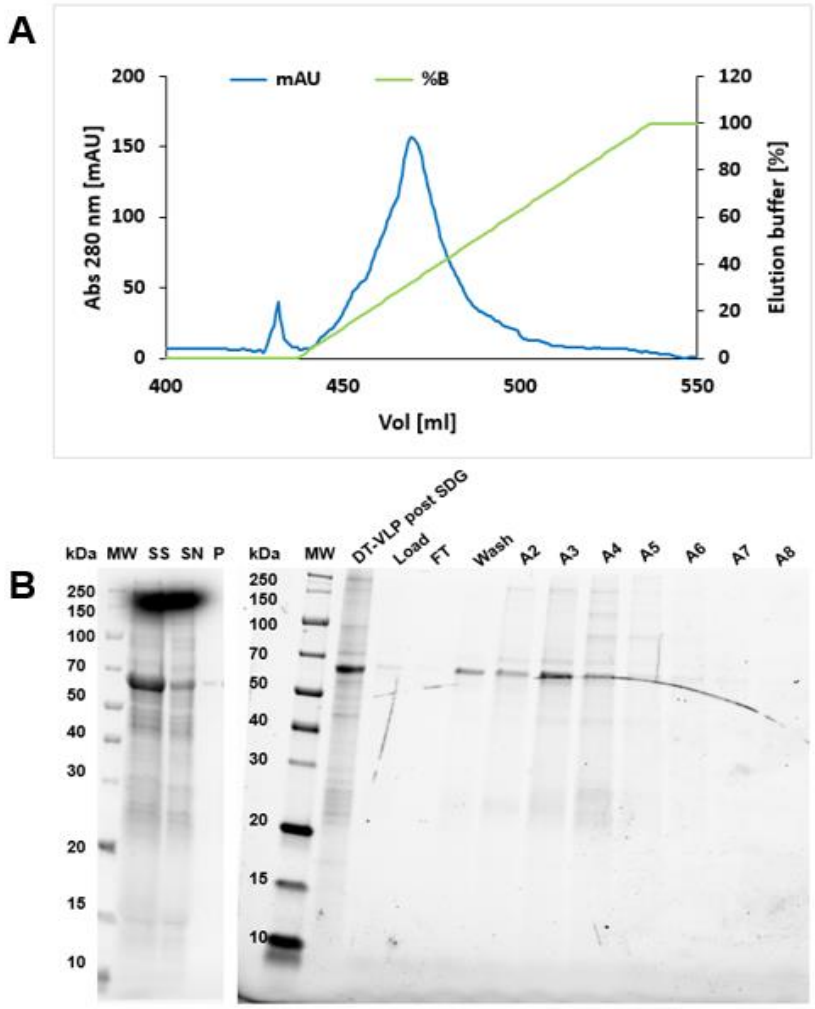

Figure 10. *Purification of DogTag-noroVLP.* ***A)*** *IEX chromatogram after applying linear salt gradient elution (green line). The protein absorbance (280 nm) curve is illustrated as a blue line.* ***B)*** *SDS-PAGE results of Stain-free gels from both purification steps. On the far-left side, a small part of the gel image shows the start sample (SS), supernatant (SN), and pellet (P) samples after sucrose gradient centrifugation (12 µL/well). The next gel image shows the data from samples taken after IEX purification (10 µL/well). A high concentration of noroVLPs is visible in A2, A3, and A4 fractions (highest elution peak). A sample of DogTag-noroVLP after sucrose gradient is also included as "DT-VLP post SDG" (2 µL). The images were taken with ChemiDoc XRS+.*

5.3.3 Size, homogeneity, and stability measurements

The size and homogeneity of DogTag-noroVLP were estimated by dynamic light scattering (DLS). The analysis result showed a hydrodynamic diameter of 58.09 nm (± 0.12) (Figure 11), and a polydispersity index (PdI) of 0.22. The hydrodynamic diameter

value represent the arithmetic mean obtained from three measurements with a standard deviation (±).

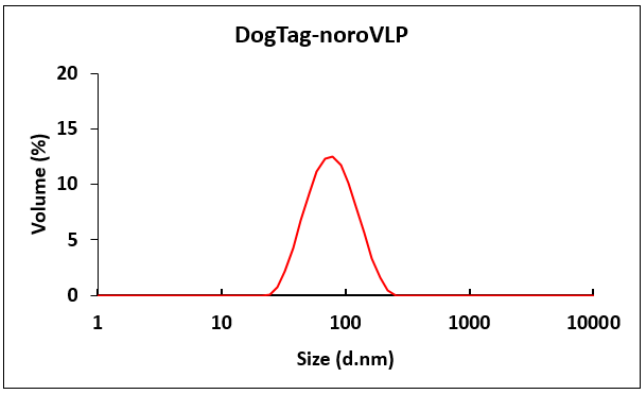

Figure 11. *DLS results for DogTag-noroVLP. The hydrodynamic diameter was estimated to be 58.09 nm (± 0.12).*

Differential scanning fluorimetry (DSF) measurement was conducted to examine DogTag-noroVLP stability and melting temperature (T_m). SpyTag-noroVLP and WT-noroVLP were included in the same measurement as control and for comparison. The value of melting temperature was obtained from the arithmetic means of three independent measurements with a standard deviation (±). Melting temperature of DogTag-noroVLP was estimated to be 61.3 °C (± 0.40), while SpyTag-noroVLP and WT-noroVLP had 64.9 °C (± 0.40) and 66.4 °C (± 0.48) respectively.

5.4 Coronavirus antigens fused with SnoopTagJr

5.4.1 Production of SnoopTagJr-antigens

SnoopTagJr-RBD (Receptor-binding domain) and SnoopTagJr-RBM (Receptor-binding motif) were utilized in this project as coronavirus (SARS-CoV-2) antigens to test conjugation reaction with DogTag-noroVLP. SnoopTagJr-RBM and 5FAM-SnoopTagJr-RBM (15 mg/mL) were both chemically synthesized by a commercial provider, with purity > 94%. The proteins were delivered in lyophilized form and were resuspended according to the provider´s instructions.

SnoopTagJr-RBD protein was produced the same way as DogTag-noroVLPs with a baculovirus expression system. Hi5 cells (viable > 95%) were infected with different MOI values (0.5, 1, 1.5, 2, 2.5) of P3 baculovirus stocks. After 6 days of incubation, protein samples were collected and prepared for purification. Start sample was taken from each culture for SDS-PAGE and WB analysis (Figure 12). SnoopLigase and SnoopTagJr-RBD

(MOI 0.5 production previously purified and concentrated) were included as a positive control for WB since we used mouse anti-histidine antibody for detection of SnoopTagJr-RBD in Start samples (SS). SnoopTagJr-RBD protein band on images matches the theoretical MW (~30kDa) that was estimated with the ProtParam tool (https://web.expasy.org/protparam/; 27.5.2020). The appearance of SnoopTagJr-RBD has a fuzzy appearance on SDS-PAGE (Figure 12A) and WB (Figure 12B). Western blot data confirmed the presence of both positive controls and SnoopTagJr-RBD in some start samples. The second band of SnoopTagJr-RBD alone and SnoopLigase indicates the presence of dimers, since their MW is doubled.

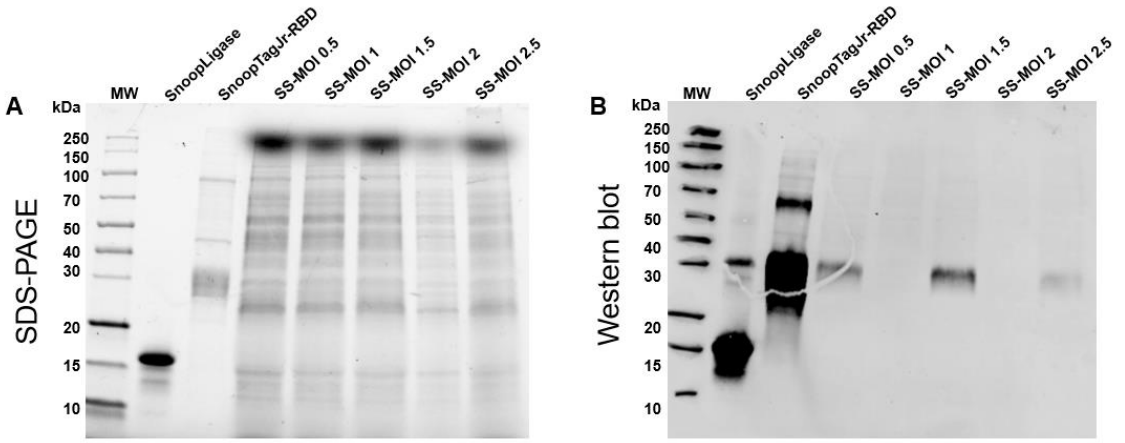

Figure 12. *Characterization of SnoopTagJr-RBD production cultures.* ***A)*** *SDS-PAGE results of production cultures made with different MOI values. "SS" stands for start sample obtained from product collection before purification preparation. SS samples (13 µL/well) were loaded onto Stain-free gel and imaged with ChemiDoc XRS+.* ***B)*** *For Western blot analysis we utilized mouse anti-histidine antibody to detect the presence of both positive controls and SnoopTagJr-RBD. Odyssey CLx system was used to obtain the image.*

5.4.2 SnoopTagJr-RBD purification

Purification of SnoopTagJr-RBD was performed based on the presence of 6xHistidine Tag. The first elution attempt included a loading sample of one production culture of 200 mL (MOI 0.5) and elution based on linear imidazole gradient (20 to 500 mM). Obtained data revealed that the absorbance (280 nm) curve was almost flat which indicated a low protein concentration in elution fractions (data not shown). According to these results, we made a one-step elution protocol that applies a constant concentration of imidazole (0.4 M) (Figure 13A). Different MOIs productions were pooled together and purified at the same time, in order to obtain more concentrated protein samples. After purification, all samples were collected and analysed with SDS-PAGE (Figure 13B) and Western blot (Figure 13C). The protein absorbance 280 nm curve shows one clear peak where all proteins get eluted (Figure **13**A). SnoopTagJr-RBD cannot be detected clearly

in SDS-PAGE image due to the presence of impurities that most likely got eluted at the same time. Western blot data included SnoopTagJr- RBD from the first production as a positive control. There are two bands visible in all protein samples that indicate the existence of dimers since it matches the double size of SnoopTagJr-RBD. Protein purity was estimated to be between 60-80% depending on the different production batches and the yield of ~6 mg/L.

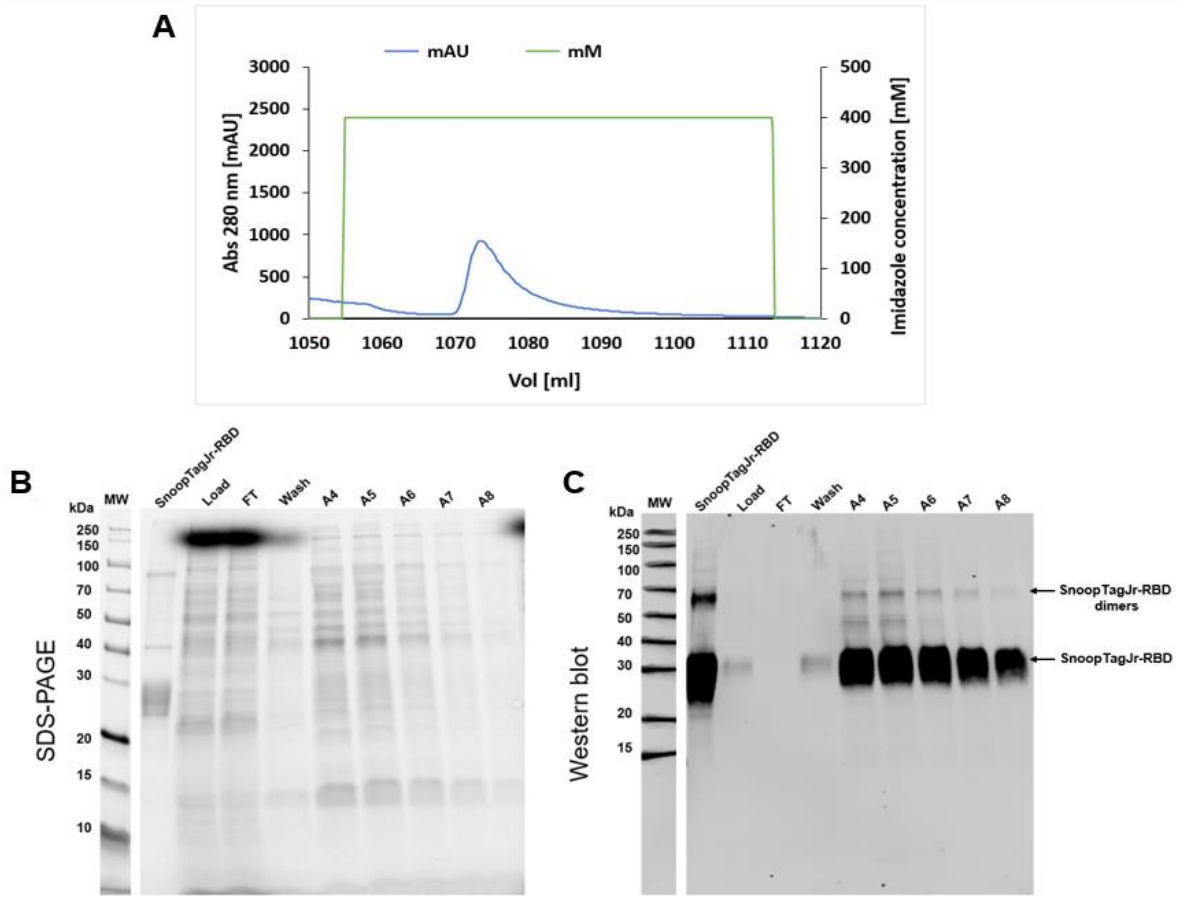

Figure 13. *SnoopTagJr-RBD purification.* ***A)*** *IMAC chromatogram data after one-step elution with a constant concentration of imidazole (green line). The protein absorbance (280 nm) curve is illustrated as a blue line.* ***B)*** *SDS-PAGE image of Stain-free gel includes Load, FT, Wash, and peak elution samples (A4-A8) (10 µL/well). The image was obtained with ChemiDoc XRS+.* ***C)*** *Western blot data included SnoopTagJr-RBD from the first production as a positive control. Mouse Anti-HisTag antibodies were used to detect SnoopTagJr-RBD in samples. There are two bands visible in all protein samples that indicate the existence of dimers since it matches the double size of SnoopTagJr-RBD. Furthermore, in A4 and A5 at least 3 different protein bands were observed. The image was taken with Odyssey CLx system.*

5.5 Conjugation reactions

The conjugation reaction experiments included DogTag-noroVLPs, SnoopTagJr-coronavirus antigens, and SnoopLigase. After production and purification of each

component, we wanted to test the ability of (biotinylated) SnoopLigase to catalyse isopeptide bond formation between DogTag-noroVLPs and SnoopTagJr-antigens in different sets of conditions in order to decorate noroVLPs. The aim was also to establish the most favourable environment for the achievement of the highest conjugation efficiency.

5.5.1 DogTag-noroVLP and 5FAM-SnoopTagJr-RBM

5-FAM-SnoopTagJr-RBM was used for conjugation experiments, due to the fluorescence tag that allowed clear visualization with ChemiDoc XRS+ (Bio-Rad) using Alexa Fluor 488 fluorescent blot imaging method (details in 4.1.1). SnoopTagJr-RBM is relatively small (~3.5 kDa) and therefore it would be difficult to confirm conjugation product without the 5FAM tag.

The first conjugation experiment included a standard reaction setting mixture incubated for 48 hours, with or without 15% glycerol (v/v). Based on the positive fluorescence signal, the gel image determined the presence of conjugates in the DogTag-noroVLP size range (Figure 14A left). SnoopLigase was used as a negative control since it should not give any signal due to lack of fluorescence. It is noticeable that the conjugation efficiency was certainly low in samples incubated at room temperature (RT) without glycerol. The gel was additionally incubated in PageBlue (Thermo Fisher Scientific) for total protein staining, which revealed otherwise undetectable SnoopLigase and unconjugated DogTag-noroVLPs (Figure 14A right). The second conjugation experiment was executed with the same reaction mixture setting, this time incubated for 24 hours and with glycerol. The gel image on the left (Figure 14B left) shows a lack of signal for conjugates particles, hence we can conclude that the conjugation efficiency was much lower than the 48-hour reactions. This can be verified with the image on the right side (Figure 14B right), where strong band intensity demonstrates the DogTag-noroVLPs (mostly unconjugated) compared to the weak fluorescence signal present on the image on the left side. DogTag-noroVLP was also included as a negative control. According to the obtained data, the optimal incubation period for conjugation to occur between these components would be 48 hours.

Another experiment included standard incubation conditions with glycerol (48h) and constant concentration of DogTag-noroVLP mixed with various molar ratios of SnoopLigase and 5FAM-SnoopTagJr-RBM (Figure 14C). The data shows that the

conjugation reactions were successful with 2-fold molar excess of SnoopLigase/5FAM-SnoopTagJr-RBM and more, and there was no apparent difference between those.

The conjugation efficiency of differently biotinylated SnoopLigase (SL) was investigated in a standard reaction setting. SnoopLigase biotinylated with BirA (BirA-SL), 20-fold NHS-Biotin (20F NHS-SL), 10-fold NHS-Biotin (10F NHS-SL) and 5-fold NHS-Biotin (5F NHS-SL) were tested separately. The conjugated particles were visible in all the samples, with an equal conjugation rate (Figure 14D).

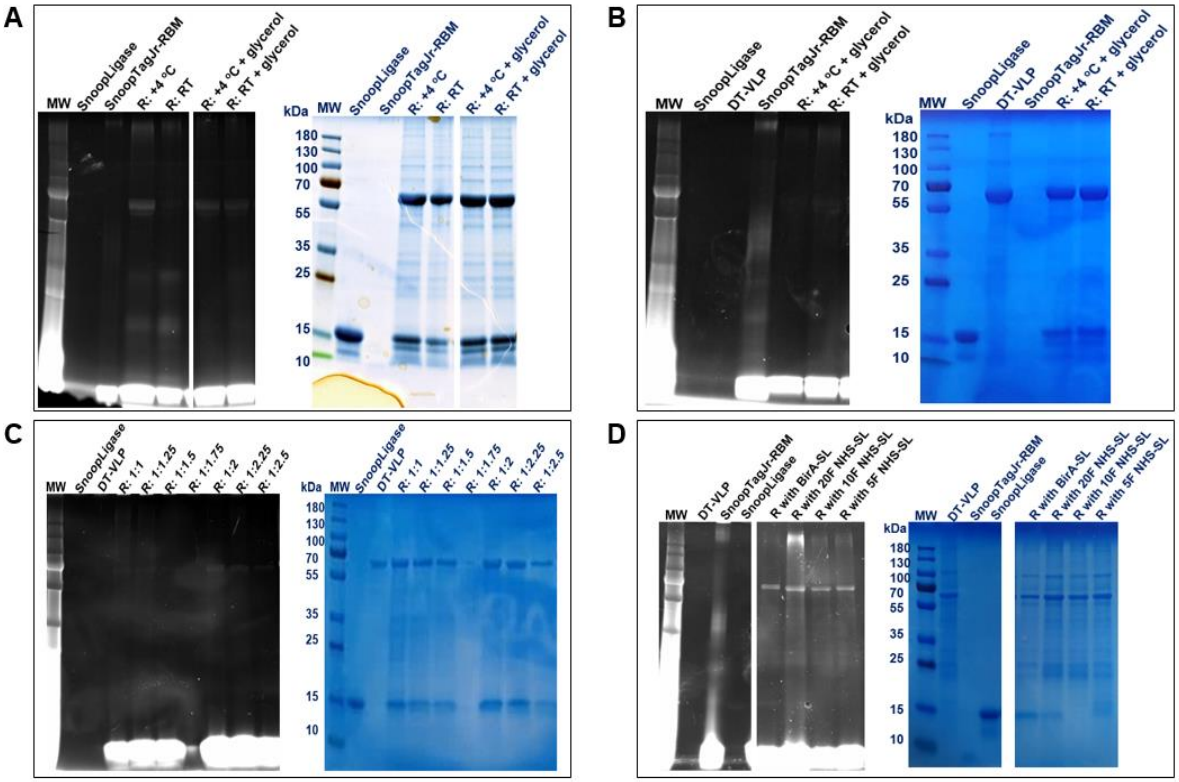

Figure 14. *Conjugation reactions between DogTag-noroVLPs and 5FAM-SnoopTagJr-RBM.* ***A)*** *Reactions incubated for 48 hours. Conjugated particles emit fluorescence signal visible on the gel image (left) and all proteins are visible with PageBlue staining (right image). "R" is short for the reaction mixture, after which the incubation temperature (+4 °C or RT) and presence of glycerol is indicated.* ***B)*** *Reactions incubated for 24 hours with the same annotations as previous images.* ***C)*** *Reactions with a constant concentration of DogTag-noroVLPs and a various molar excess of SnoopLigase and 5FAM-SnoopTagJr-RBM.* ***D)*** *Reactions with differently biotinylated SnoopLigase. SnoopLigase biotinylated with BirA (BirA-SL), 20-fold NHS-Biotin (20F NHS-SL), 10-fold NHS-Biotin (10F NHS-SL), and 5-fold NHS-Biotin (5F NHS-SL) were tested separately. All samples (11 µL/well) were loaded onto Pre-stained gel, imaged with ChemiDoc XRS+ (Alexa 488) and then incubated in PageBlue.*

The DogTag-noroVLPs conjugated with 5FAM-SnoopTagJr-RBM were imaged with TEM in order to assess their morphological characteristics (Figure 15).

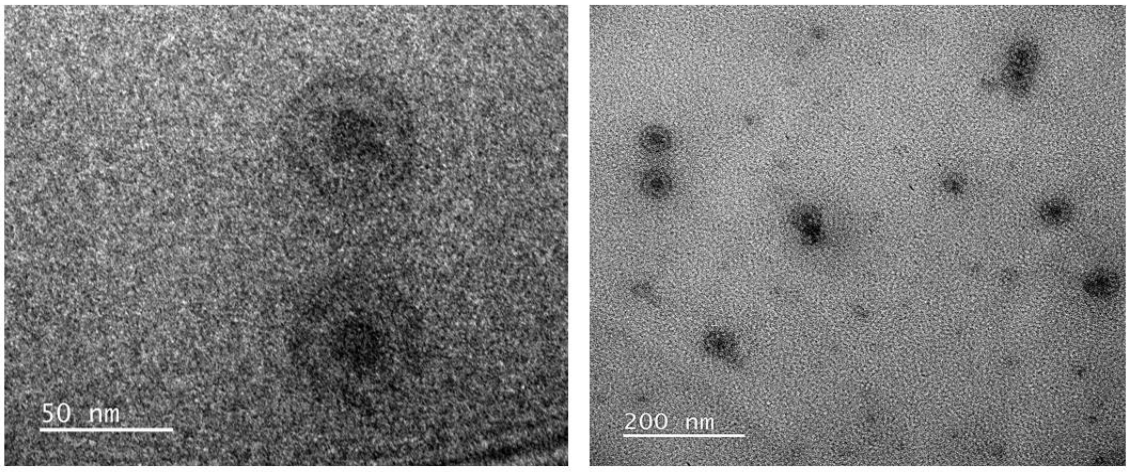

Figure 15. *TEM images of conjugation complex between DogTag-noroVLP and 5FAM-SnoopTagJr-RBD. The morphology of the particles looks the same as observed with other noroVLPs [10]. It is not possible to detect conjugation partners or tags.*

5.5.2 DogTag-noroVLP and SnoopTagJr-RBD

The reaction experiments with DogTag-noroVLP and SnoopTagJr-RBD followed the standard reaction setting. We tested the effect of glycerol on conjugation rate, incubation for 24 or 48 hours, and in 50 mM PBS pH 7.5. The results were analysed with SDS-PAGE (stain-free) and Western blot using anti-histidine antibodies (section 4.5.1). First reaction mixtures were incubated for 48-hours with/without 15% glycerol (v/v) at different temperatures. The conjugate bands are visible at the ~91 kDa on the SDS-PAGE image (Figure 16A left). This was confirmed with Western blot results (Figure 16A right), where only reaction samples gave a positive signal for the presence of SnoopTagJr-RBD at that level, while the negative control (DogTag-noroVLP) was not detected. We can also notice an absence of the second band in DogTag-noroVLP in SDS-PAGE, which can further confirm the success of conjugation. For the second trial, reaction settings were the same with additional reactions incubated in PBS. Based on the given results (Figure 16B), it is noticeable that the conjugation progress was almost equal in the 24 hours as with 48 hours. The conjugation efficiency rate was estimated to be ~20%, and it was analysed as explained in 4.5.1. We were able to confirm that glycerol can indeed enhance reactions, especially those incubated at room temperature. The reactions in PBS were not fruitful, despite the presence of glycerol.

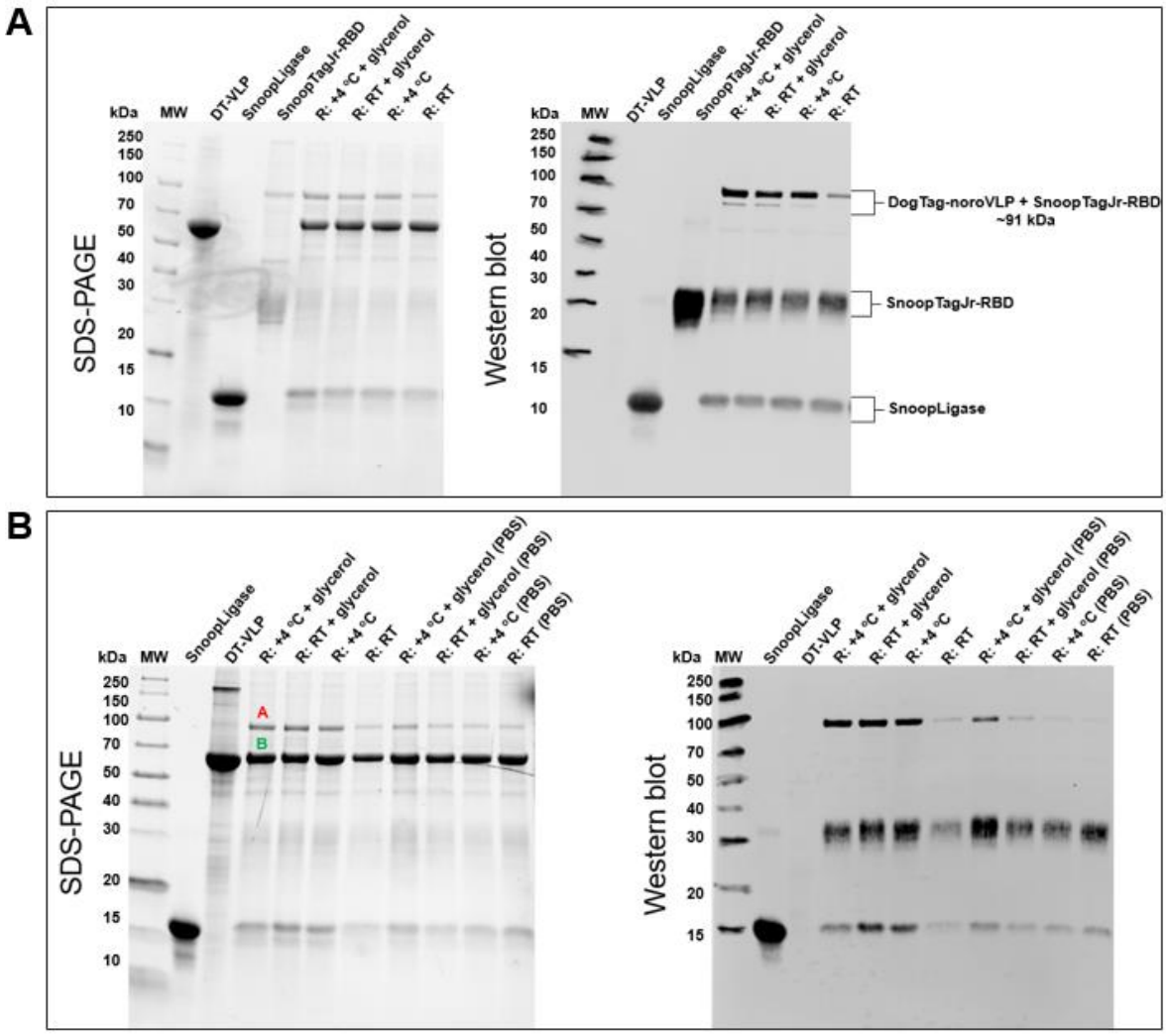

Figure 16. *Conjugation reactions between DogTag-noroVLPs and SnoopTagJr-RBD.* ***A)*** *SDS-PAGE data (left) for reactions incubated for 48 hours. Conjugates visible at ~91 kDa. Western blot data (right) confirms the presence of conjugates by recognition of SnoopTagJr- RBD using Anti-HisTag antibodies.* ***B)*** *SDS-PAGE results (left) for reactions incubated for 24 hours. Estimation of conjugation efficiency was done by comparing the % of conjugated particles (A) with the % of unconjugated (B) when the total proportion of all particles is 100%. Western blot result shows the conjugation products. All conjugation samples were loaded in same volume (11 µL/well), SDS-PAGE and WB images were obtained the same as usual.*

5.5.3 Control reactions

Control reactions were set by utilizing SnoopTagJr-MBP and DogTag-MBP obtained from Howarth´s lab (University of Oxford). We tested the reactions between SnoopTagJr-MBP with two types of DogTag-noroVLPs and DogTag-MBP. (Biotinylated) SnoopLigase made in our lab was used to catalyse the formation of complex and results were assessed with SDS-PAGE (Figure 13). The conjugation efficiency between SnoopTagJr-MBP with DogTag-noroVLPs (DT-VLP) was ~38.5%, which is significantly better than

with SnoopTagJr-RBD. The other type of DogTag-noroVLP that showed visible aggregations in the tube (DT-VLP VisAgg) was also tested. The SDS-PAGE result showed the existence of a third (~55 kDa) and a fourth band (~4 kDa), and the absence of conjugation complex, as well as SnoopLigase. Biotin- SnoopLigase (SL) was also efficient in forming the conjugation complex and the reactions between SnoopTagJr-MBP and DogTag-MBP were also successful. The conjugation complex was made with DogTag-noroVLP and SnoopTagJr-MBP as visible at ~95 kDa (Figure 17)

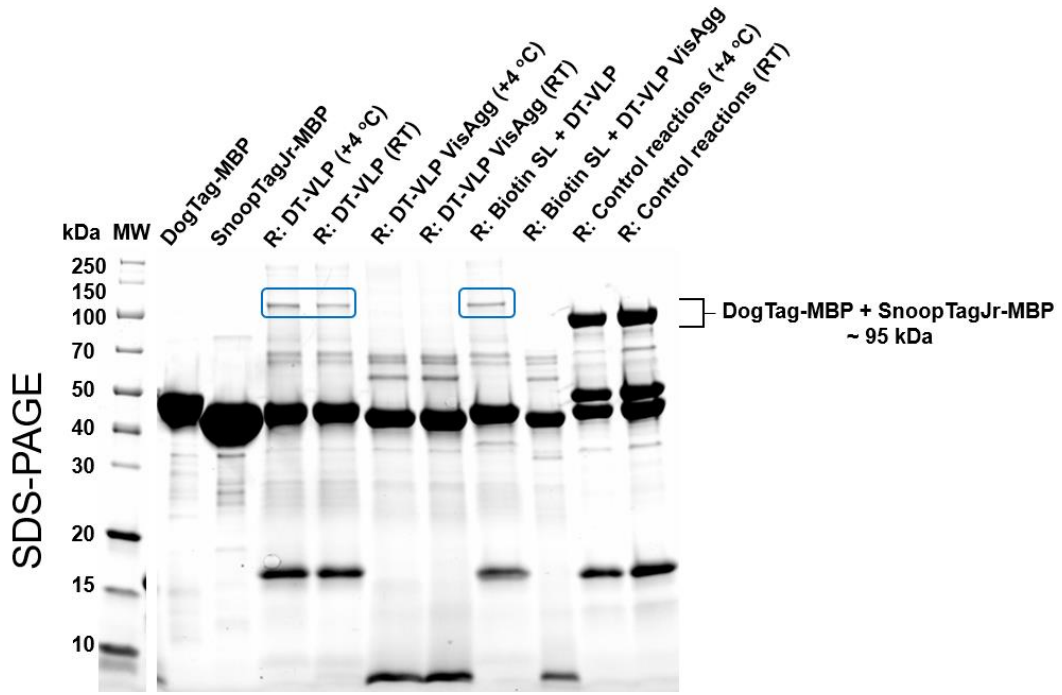

Figure 17. *Control reactions with SnoopTagJr-MBP and DogTag-MBP. SDS-PAGE image of Stain-free gel obtained with ChemiDoc XRS+. Reaction mixtures (11 µL/well) were indicated as "R" with the incubation conditions and composition. Biotin SL represents biotinylated SnoopLigase (with BirA). The conjugation complex formed between DogTag-noroVLPs and SnoopTagJr-MBP is indicated by the blue square.*

5.5.4 Removal of the SnoopLigase

The removal trial was done as described in section 4.5.2. All samples collected during and after the process were analysed with SDS-PAGE (Figure 18). The reaction mixtures were divided into two samples to make a replicate (I and II). The result data indicates that most of SnoopLigase gets eluted already after incubation with streptavidin resin. The results from the following steps indicates that the conjugation complex gets eluted together with SnoopLigase. In the elution products, the presence of all components is still visible but in the low concentrations. Resin samples don´t have any trace of SnoopLigase, which means that no protein is bound to it.

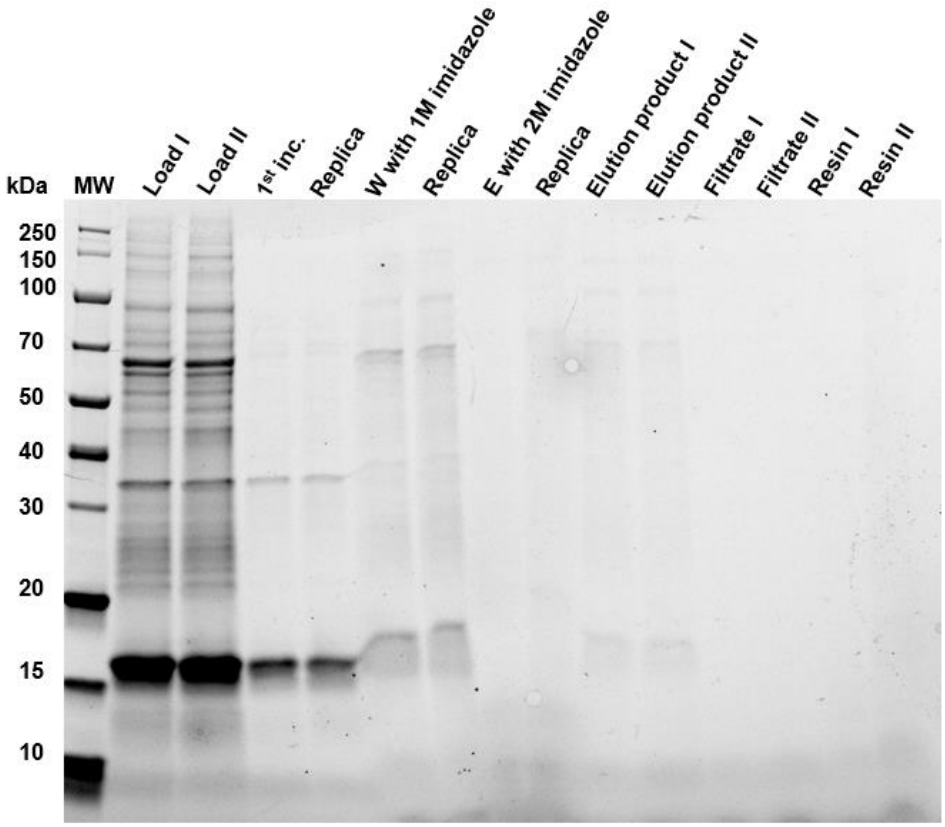

Figure 18. *Removal of SnoopLigase from conjugation complex. Samples (11 µL/well) loaded onto Stain-free gel and the image was obtained with ChemiDoc XRS+. Two parallel reaction tubes were included into experiment (I and II or replica). Washing step is marked as "W" and Elution step as "E".*

6. DISCUSSION

6.1 SnoopLigase

AviTag-SnoopLigase plasmid transformation and production were successful in bacterial cells. We primarily followed the well-established protocols described in published research papers [8,63]. The optimum time for expression of SnoopLigase was estimated to be four hours. Additionally, we also included over-night production cultures into this study to make a comparison and observe if there is any difference in production yield after purification.

The purification of SnoopLigase was accomplished with the IMAC purification method using the stepwise imidazole concentration. Based on the chromatogram (Figure 7B), most of the impurities get eluted after the first increase of imidazole (125 mM), while SnoopLigase elutes after the second imidazole increase (350 mM). With SDS-PAGE and WB, SnoopLigase was detected at a molecular weight of 15.4 kDa (Figure 7A), which matches its predicted theoretical molecular weight. In general, the purity level of SnoopLigase was indeed very high (~90%) taking into consideration all the production cultures and therefore there was no need for another round of purification. In Figure 7C and some other SDS-PAGE/WB images, there is also a second band detected at ~30 kDa in SnoopLigase samples. Since it matches the double weight of SnoopLigase, it most likely represents SnoopLigase dimers. This phenomenon has not been reported previously, however, it only happens to appear in highly concentrated samples. It also doesn´t seem to influence SnoopLigase performance or stability.

6.1.1 Biotinylation of SnoopLigase

Biotinylation of SnoopLigase was conducted with two different methods, and both of them showed promising results. The main goal was to get exactly one or more biotins per SnoopLigase molecule. The purpose of biotinylated SnoopLigase besides conjugation is to bind streptavidin resin to test the removal of the SnoopLigase from the conjugation product. The SnoopLigase gets immobilized on the resin due to the strong interaction between biotin and streptavidin molecules, and such enables the elution of the conjugates while SnoopLigase stays bound to the resin.

The first method involved non-specific (chemical) biotinylation with various molar excess fold (5 to 20) of NHS-PEG_{12}-Biotin reagent. The PEG_{12}-biotin molecule can bind to every lysine amino acid present on SnoopLigase (10 in total), which is displayed on the gel as the protein band shift upwards. The binding of biotin is quite heterogenous, since not every molecule gets the same amount of biotin attached. The differences in protein band shift between different fold samples indicate the variations in biotinylation efficiency. Also, PEG_{12}-Biotin moiety does not bind sodium dodecyl sulphate (SDS) and it also neutralizes the charge of Lysine residues, reflecting into intrinsic charge of the protein. That can cause the mass-to-charge ratio which affects the mobility of the protein. Based on SDS-PAGE results (Figure 8A) the biotinylation with the 15- and 10- fold NHS-PEG12-Biotin were the most successful, in which every SnoopLigase molecule appears to be biotinylated with several biotin molecules. On the contrary, the 20- and 5- fold samples appear to have some unbiotinylated molecules. To our knowledge, this is the first reported experiment about the chemical biotinylation of SnoopLigase.

The second method of biotinylation included bacterial BirA enzyme [93], which binds only one biotin molecule to the specific site on AviTag. This method was previously utilized for SnoopLigase biotinylation [8]. The attachment of one biotin was difficult to determine with only SDS-PAGE, however, Western blot results provided solid evidence on biotinylated SnoopLigase (Figure 8B). First, we incubated the samples with CNCA avidins that recognize and bind biotin if present on the protein, then we used anti-avidin antibodies for recognition of avidin and conformation of biotinylation. Based on the comparison of SDS-PAGE (data not shown), and WB data, it is safe to assume that the majority of SnoopLigase gets biotinylated using BirA enzyme. In addition, the precise estimation of the number of biotin molecules coupled to SnoopLigase or determination of successful biotinylation can be done in the future with HABA (4'-hydroxyazobenzene-2-carboxylic acid) assay.

6.2 DogTag-norovirus-like particles

Recombinant baculovirus stocks were made in Sf9 cells, while the production of DogTag-noroVLP was accomplished in Hi5 cells that have previously demonstrated better performance and higher yield. The obtained baculovirus stock titers weren´t high, however, all the DogTag-noroVLPs were made successfully from the same batch. The construct of DogTag-noroVLP is based on the same construct used in previous studies [10,72], with the substitution of SpyTag with DogTag. In these studies, it has been concluded that the MOI values of 1 and 0.5 appear to be optimal to produce noroVLPs.

Similar results were obtained in this research project. Based on Figure 9 there was no noticeable difference between production cultures from different MOI values, however, production cultures from MOI 1 and 0.5 seemed to have fewer impurities and were quite pure after the first purification step.

The unexpected result was the appearance of DogTag-noroVLP as one band on the SDS-PAGE and Western blot. The double band visible in the SpyTag-noroVLP sample (used as a positive control) is a common trait of noroVLPs VP1 that undergoes posttranslational cleavage of N-terminal fragment (3.4 kDa) [70]. Some DogTag-noroVLPs appeared as a double band on the SDS-PAGE gel (Figure 17) when present in lower concentrations. However, the double band is not as visible as with other noroVLPs of the same construct. It is also necessary to reflect that this was the first time that the *flash*BAC ULTRA baculovirus system was used for producing noroVLPs. In previous studies, the norovirus-like particles (genotype GII-4) were produced with a Bac-to-bac baculovirus expression system and the optimum period for VLPs expression was 5-6 days [10,57,70,71]. The *flash*BAC ULTRA baculovirus system has a certain proteases deleted in the baculovirus genome compared to the Bac-to-bac system and maybe those are important for processing of noroVLPs. Nevertheless, more studies need to be performed to examine this occurrence.

The purification of DogTag-noroVLPs was conducted as described for the SpyTag-VLPs [10]. The hypothesis was that the same purification methods would work similarly for the DogTag-noroVLPs since the constructs are almost identical. The results obtained were as expected, the samples were quite pure after the sucrose-gradient purification and also some amount of DogTag-noroVLPs is eluted during the wash step in IEX. Overall, the purity of the DogTag-noroVLPs was between 80-95%, combining all the production cultures. The estimation of DogTag-noroVLP production yields was ~16 mg/L, which is similar to SpyTag-noroVLPs (10-30 mg/L) [10] and much better than HisTag-noroVLPs (1.5 mg/L) [57]. The DogTag-noroVLP were stored at +4 °C, endotoxin-free in PBS. However, they were stable for only one month, unlike SpyTag-noroVLPs that were stable for months in same conditions. After one month, the solution with DogTag-noroVLPs would get hazy/yellowish, and on the SDS-PAGE it appeared as a three-band DogTag-noroVLP (Figure 17). Originally, we thought that the samples might have gotten contaminated somehow, but after the second mass-production the samples were carefully sterilized and kept without further handling. These samples also were stable for only one month. This occurrence happens to be the case with the samples that were purified with only sucrose-gradient centrifugation. Since the samples were not purified

with IEX, it is possible that some insect proteases remained in the sample and cause this effect after a certain amount of time.

In further studies, I would suggest the testing of different storage conditions. For example, examination of the effects of lower temperature on particle stability (-20 °C or -80 °C) and/or the addition of some preservative agents. Since the potential problem might be the presence of proteases, including the protease inhibitors into storage buffer might be a plausible solution. Another approach would be to do the re-design of the DogTag-noroVLP construct and try the Bac-to-bac baculovirus expression system. Nevertheless, the automatized mass-production and purification of DogTag-noroVLPs for vaccine usage is also possible with the current construct.

6.2.1 Size, homogeneity, and stability

The size of the DogTag-noroVLP is estimated to be around 58 nm. The particle size is slightly bigger than the SpyTag-noroVLP (~50 nm) [10], probably due to the larger size of the DogTag. The polydispersity index (PdI) of 0.22 indicated the monodispersed particles [100].

The results from thermal stability measurements (DSF) showed that the T_m of DogTag-noroVLP is slightly lower than the SpyTag-noroVLP and WT-noroVLP constructs, however, the difference was not significant. Since the DogTag is larger than SpyTag, this may destabilize noroVLP more. It has been already reported that the decoration of native noroVLP with SpyTag and antigen can impair its stability to a small extent [10].

6.3 Coronavirus antigens fused with SnoopTagJr

SnoopTagJr-RBM and 5FAM-SnoopTagJr-RBM (5 mg/mL) were made by a commercial provider, delivered in lyophilized form, and resuspended according to the provider´s instructions.

SnoopTagJr-RBD was produced in the same manner as DogTag-noroVLPs, using a baculovirus expression system. Even though the baculovirus titers results were good, the production yield was much lower than expected. Therefore, the baculovirus P3 stock was produce twice to meet the production needs. According to the SDS-PAGE and WB analysis from start samples (Figure 12), SnoopTagJr-RBD was detected at the expected molecular weight of ~30 kDa, and the production with MOI: 1.5 seems to be most fruitful. The SnoopTagJr-RBD was not detected in samples with MOI: 1 and 2, most likely due

to some technical issues like improper sample collecting or pipetting. The fuzzy appearance of SnoopTagJr-RBD band in PAGE is expected due to the existence of diverse glycoforms on the N-terminus glycosylation sites [101]–[103]. Glycosylation increases protein solubility and stability, as well as helping to evade host immune response by hiding the immunogenic epitopes on S protein [102]. The glycosylation of SnoopTagJr-RBD can also be tested by different methods, such as enzymatic/chemical cleavage of glycans, staining procedures, or affinity-based procedures [104].

After the first IMAC purification using linear imidazole gradient elution, the concentration of SnoopTagJr-RBD was very low, but the purity levels were alright (Figure 13B, SnoopTagJr-RBD sample). Following purifications included one-step gradient elution, where we obtained more concentrated protein samples with much lower purity (Figure 13B). Since we utilized a one-step elution procedure, most likely all bound proteins got eluted from the column at the same time, including impurities. In the WB results (Figure 13C), in all samples there happens to be one or two bands detected beside SnoopTagJr-RBD. The band at ~60 kDa indicates the presence of dimers, which was also observed in previous studies with RBDs from Spike glycoprotein [30]. The middle band might appear due to non-specific antibody binding since this has only been observed in this WB result and in highly concentrated samples that contain some impurities. Overall, the purity of SnoopTagJr-RBD was estimated to be between 60-85% depending on the different production batches and the yield of ~6 mg/L.

Based on the results, the optimal method for SnoopTagJr-RBD purification is the elution with linear imidazole gradient since it provided the purest protein samples, however, a two/three-step elution method can also be applied. To improve SnoopTagJr-RBD production, there are a few options that can be tested in the future. One of them is the production of the completely new recombinant baculovirus stocks, starting from the P1 stock or even trying some other type of baculovirus expression systems like Bac-to-bac or BestBac. One study reported a yield of 30 mg/L of 95% pure RBD protein domain, using the BestBac system and MOI 5 [105]. Another way is to optimize production conditions, such as harvesting the production cultures in less than six days post-infection and to try infection with higher MOI values. The reported yield of purified SpyTag-RBD obtained with mammalian expression system was 100 mg/L, which is considerably higher than the results we had with the baculovirus expression system. Therefore, an additional approach would be to try producing SnoopTagJr-RBD in mammalian cells. It is also plausible to try production of nucleocapsid protein (N) fused with SnoopTagJr, which has been showed to be highly conserved and immunogenic antigen [106].

6.4 Conjugation reactions

6.4.1 DogTag-noroVLP and 5FAM-SnoopTagJr-RBM

The conjugated DogTag-noroVLPs with 5FAM-SnoopTagJr-RBM were detected with the fluorescent blot imaging method. The negative control (just DogTag-noroVLP) and unsuccessful conjugation reaction are identified through the lack of fluorescent signal in the DogTag-noroVLP area, but their presence was verified with PageBlue total protein staining. Based on the obtained results, the optimum reaction setting includes DogTag-noroVLPs (5 µM) and the two-fold molar excess of 5FAM-SnoopTagJr-RBM and SnoopLigase incubated for 48 hours (Figure 14A, C). In this project, we also confirmed the statement that glycerol can enhance conjugation efficiency, as reported in previous studies [8]. The samples incubated with glycerol at room temperature showed much better results than the samples without glycerol (Figure 14A). The conjugation reactions with the differently biotinylated SnoopLigase were successful. The sample of SnoopLigase biotinylated with 15-Fold of NHS-PEG12-Biotin reagent got lost in the dialysis process, and therefore it was not included in the conjugation test. However, since all the other chemically biotinylated SnoopLigase enzymes were efficient in catalysing the conjugation, it is safe to assume that the 15-Fold samples would work the same.

The morphology of DogTag-noroVLPs conjugated with 5FAM-SnoopTagJr-RBD was visualised with TEM (Figure 15). The morphology of the particles is the same as observed with the other noroVLPs [10]. It was not possible to detect conjugation partners or tags.

6.4.2 DogTag-noroVLP and SnoopTagJr-RBD

The conjugation between DogTag-noroVLPs and SnoopTagJr-RBD was detected with SDS-PAGE and Western blot at ~91 kDa band (Figure 16). There was no apparent difference between the 24- and 48-hours incubation period. For the more representable comparison, 24- and 48-hour reaction products should have been placed on the same gel next to each other. The conjugation efficiency rate was estimated to be ~20%, which is notably lower compared to results obtained with coupling of IMX-nanoparticle with small peptide epitope using SnoopLigase (~78%) [9], as well as influenza antigens and SpyCatcher-VLP system (~50%) [10]. We were again able to confirm the benefit of glycerol on conjugation reaction at room temperature. The reactions incubated in PBS provided poor results, even in the presence of glycerol. Therefore, Tris-borate (50 mM, pH 7.5) buffer seems to work the best for this purpose.

During this project, we could not complete all planned experiments successfully, due to the occurrence of certain challenges we came across, such as DogTag-VLP short-term stability and SnoopTagJr-RBD poor production yield. Some production cultures were also not very viable. For future studies, I would suggest testing a different pH values of reaction buffer on conjugation efficiency and perhaps incubation at various time intervals to optimize reaction settings ever further.

6.4.3 Control reaction

Control reactions included the SnoopTagJr-MBP and DogTag-MBP proteins that we acquired from Howarth´s lab (Oxford). We tested conjugation with (biotinylated) SnoopLigase and DogTag-noroVLPs. The decoration of DogTag-noroVLP with SnoopTagJr-MBP was successful, with a conjugation efficiency of around 38.5% which is significantly better than with SnoopTagJr-RBD. This implicates that there may be some issues with SnoopTagJr-RBD that affects the conjugation results. We also confirmed the efficiency of biotinylated (BirA) SnoopLigase to form a conjugation complex. The conjugation between DogTag-MBP and SnoopTagJr-MBP was also successful and visible at ~95 kDa (Figure 17).

In the samples with DogTag-noroVLP that showed visible aggregation, there is third band present near DogTag-VLP and the fourth band near 5 kDa. A similar event was observed in some SpyCatcher-M2e samples upon reaction in the experiments done in our lab (data not published). This truncation of VLPs can be explained by the presence of some insect/baculovirus proteases left in the samples that were not purified additionally with IEX. In some other SDS-PAGE images (data not presented), SnoopLigase is visible in the samples with three-banded DogTag-noroVLPs, however, it appears as a two-band. It might be that the SnoopLigase gets affected by proteases as well and gets degraded or interacts with the degraded parts of DogTag-noroVLP. To our knowledge, this type of behaviour has not been reported in previously published research papers. Nevertheless, this phenomenon needs to be investigated thoroughly in order to make a relevant conclusion.

6.4.4 Removal of the SnoopLigase

The removal of the biotinylated SnoopLigase from the conjugation complex was mostly done as reported in previous studies [8,63], with the slight adjustments in imidazole concentration since the experiment performed in our lab (data not published) indicated

that the high concentration of imidazole can alter the stability of noroVLP. The SDS-PAGE results showed that most of the SnoopLigase got eluted already after incubation with streptavidin resin. In the following steps, the conjugation product was eluted together with SnoopLigase. Also, streptavidin resin didn´t contain any trace of SnoopLigase which means that SnoopLigase didn´t bind the resin at all. These poor results implicate either problem with biotinylated SnoopLigase or malfunctions of streptavidin resin. However, during this project, we did not validate these hypotheses.

Based on the outcome, this process needs to be heavily optimized, and unfortunately, there was not enough time to do so in this thesis project. There are a couple of experiments that can be tried in future. One of them is to try new streptavidin resin and test binding of biotinylated SnoopLigase alone to ensure it works properly. It would be beneficial to attempt removal experiments with chemically biotinylated SnoopLigase since there are more biotins attached and it can potentially bind resin more firmly. The elution of the conjugation complex can be tested using the peptide elution; however, this approach is costly and more time-consuming, especially for mass production.

Another important element needs to be taken into consideration after successful removal of SnoopLigase. Stability measurements need to be conducted for each conjugation product since there is no information on how long the conjugates can be stable at certain temperatures and in different conditions. This information is crucial for vaccine storage and shelf-life.

6.5 Other perspectives

If the whole process gets successfully optimized, the next big step is to start pre-clinical studies in mice. It is important to investigate whether this vaccine can elicit a solid immune response and to determine the immunogenicity of both the RBD domain and RBM peptide. Andersson *et al* reported that the depletion of SnoopLigase from the conjugation complex did not have a significant effect on the immune response to the tested pathogen [9], therefore this can also be tested with this vaccine platform. The comparison of the immune response between SpyCatcher/SpyTag and SnoopLigase noroVLP platforms could be valuable for future noroVLP-based vaccines.

One of the aims proposed in this project was the comparison between DogTag/SnoopLigase conjugated particles with directly fused norovirus-coronavirus hybrids. The production of genetically fused noroVLPs with coronavirus RBD was not

directly part of this thesis, but the experiment that was conducted in our lab. Unfortunately, this method of noroVLP decoration was not successful, most likely due to the larger size of RBD that interfered with folding and secretion. This has shown again the challenges that can come up with using genetic fusion as a decoration method. Therefore, the idea to implement the decoration of noroVLPs with the SnoopLigase system turned out to be a good choice since it provided much better results. Coupling of antigens to peptide tags instead of fusion to the VLPs should provide rapid and cost-effective Good Manufacturing Practice (GMP) development. Due to its resilience and robustness, I cannot see the reasons why the SnoopLigase system wouldn´t be utilized similarly to SpyCatcher technology [60].

So far, there are several approved vaccines against SARS-CoV-2 and even more in the approval phase. Based on this information, our product is far behind this process. However, due to the existence of many pathogens that can potentially cause severe epidemics and pandemics as well as the ongoing mutations in SARS-CoV-2, it is highly important to establish a modular and fast-to-produce vaccine platform that can rapidly adapt to required changes. Although we have met most of the set objectives during this project, it also left plenty of room for additional research and development.

7. CONCLUSION

Production of the SnoopLigase in bacterial cells was successful. We obtained protein samples with a high purity and excellent yield of ~20 mg/L. Both enzymatic and chemical biotinylation worked well and biotinylated SnoopLigase showed to have proper catalytic capacity. Until now, this is the first reported experiment that included chemical biotinylation of SnoopLigase.

DogTag-noroVLPs were efficiently produced in the Hi5 insect cell line, using a baculovirus expression system. The optimal MOI value was determined to ensure the most desirable expression results. The purification of DogTag-noroVLPs was successfully attained with sucrose gradient centrifugation followed by anion exchange chromatography. The estimated yield of pure DogTag-noroVLPs was 16 mg/L and the samples were stable for one month at +4 °C. Further studies might be needed to determine more suitable storage conditions or to upgrade the DogTag-noroVLP construct.

SnoopTagJr-RBM was chemically synthesized and delivered by commercial providers, while SnoopTagJr-RBD was produced similarly as DogTag-noroVLPs. The production yield of SnoopTagJr-RBD was lower than expected, as well as the purity levels compared to the other proteins made in this project. Therefore, with a couple of suggestions proposed in the discussion, the production process of SnoopTagJr-RBD needs to be optimized to obtain better results.

The DogTag-noroVLPs were successfully decorated with SnoopTagJr-SARS-Cov-2 antigens using the SnoopLigase system. The optimal conditions that enable the highest conjugation efficiency for each antigen were determined. The removal of the SnoopLigase from the end-product was not achieved, however, this process can be repeated with certain modifications. If the adjustments provide rewarding results, the next steps can include the preparation of decorated noroVLPs as a vaccine candidate for pre-clinical testing and the determination of antigens immunogenicity and existing immunity. The finalized product can provide a flexible, scalable, and cost-efficient vaccine platform.

8. REFERENCES

[1] M. Letko, A. Marzi, and V. Munster, “Functional assessment of cell entry and receptor usage for SARS-CoV-2 and other lineage B betacoronaviruses,” Nat. Microbiol., vol. 5, no. 4, pp. 562–569, Apr. 2020, doi: 10.1038/s41564-020-0688-y.

[2] “WHO Coronavirus (COVID-19) Dashboard | WHO Coronavirus (COVID-19) Dashboard With Vaccination Data.” https://covid19.who.int/ (accessed Apr. 05, 2021).

[3] N. Madhav, B. Oppenheim, M. Gallivan, P. Mulembakani, E. Rubin, and N. Wolfe, “Pandemics: Risks, Impacts, and Mitigation,” in Disease Control Priorities, Third Edition (Volume 9): Improving Health and Reducing Poverty, The World Bank, 2017, pp. 315–345.

[4] D. E. Bloom, “The value of vaccination,” *Adv. Exp. Med. Biol.*, vol. 697, pp. 1–8, 2011, doi: 10.1007/978-1-4419-7185-2_1.

[5] J. Fuenmayor, F. Gòdia, and L. Cervera, “Production of virus-like particles for vaccines,” *N. Biotechnol.*, vol. 39, no. 16, pp. 174–180, 2017, doi: 10.1016/j.nbt.2017.07.010.

[6] M. O. Mohsen, L. Zha, G. Cabral-Miranda, and M. F. Bachmann, “Major findings and recent advances in virus–like particle (VLP)-based vaccines,” *Semin. Immunol.*, vol. 34, no. September, pp. 123–132, 2017, doi: 10.1016/j.smim.2017.08.014.

[7] S. Thrane *et al.*, “Bacterial superglue enables easy development of efficient virus-like particle based vaccines,” *J. Nanobiotechnology*, vol. 14, no. 1, pp. 1–16, 2016, doi: 10.1186/s12951-016-0181-1.

[8] C. M. Buldun, J. X. Jean, M. R. Bedford, and M. Howarth, “SnoopLigase Catalyzes Peptide-Peptide Locking and Enables Solid-Phase Conjugate Isolation,” *J. Am. Chem. Soc.*, vol. 140, no. 8, pp. 3008–3018, 2018, doi: 10.1021/jacs.7b13237.

[9] A. M. C. Andersson, C. M. Buldun, D. J. Pattinson, S. J. Draper, and M. Howarth, “SnoopLigase peptide-peptide conjugation enables modular vaccine assembly,” *Sci. Rep.*, vol. 9, no. 1, pp. 1–13, Dec. 2019, doi: 10.1038/s41598-019-40985-w.

[10] V. Lampinen *et al.*, “Modular vaccine platform based on the norovirus-like particle,” *J. Nanobiotechnology*, vol. 19, no. 1, p. 25, Dec. 2021, doi: 10.1186/s12951-021-00772-0.

[11] J. F.-W. Chan *et al.*, “Genomic characterization of the 2019 novel human-pathogenic coronavirus isolated from a patient with atypical pneumonia after visiting Wuhan,” *Emerg. Microbes Infect.*, vol. 9, no. 1, pp. 221–236, Jan. 2020, doi: 10.1080/22221751.2020.1719902.

[12] K. Lalchhandama, “The chronicles of coronaviruses: the bronchitis, the hepatitis and the common cold,” *Sci. Vis.*, vol. 20, no. 1, pp. 43–53, 2020, doi: 10.33493/scivis.20.01.04.

[13] J. O. Wertheim, D. K. W. Chu, J. S. M. Peiris, S. L. Kosakovsky Pond, and L. L. M. Poon, “A Case for the Ancient Origin of Coronaviruses,” *J. Virol.*, vol. 87, no. 12, pp. 7039–7045, Jun. 2013, doi: 10.1128/jvi.03273-12.

[14] P. C. Y. Woo, Y. Huang, S. K. P. Lau, and K. Y. Yuen, “Coronavirus genomics and bioinformatics analysis,” *Viruses*, vol. 2, no. 8, pp. 1805–1820, 2010, doi: 10.3390/v2081803.

[15] R. Dijkman *et al.*, “The dominance of human coronavirus OC43 and NL63 infections in infants,” *J. Clin. Virol.*, vol. 53, no. 2, pp. 135–139, Feb. 2012, doi: 10.1016/j.jcv.2011.11.011.

[16] F. Wu *et al.*, “A new coronavirus associated with human respiratory disease in China,” *Nature*, vol. 579, no. 7798, pp. 265–269, Mar. 2020, doi: 10.1038/s41586-020-2008-3.

[17] A. Vandelli *et al.*, “Structural analysis of SARS-CoV-2 genome and predictions of the human interactome,” *Nucleic Acids Res.*, vol. 48, no. 20, pp. 11270–11283, Nov. 2020, doi: 10.1093/nar/gkaa864.

[18] A. C. Walls, Y. J. Park, M. A. Tortorici, A. Wall, A. T. McGuire, and D. Veesler, “Structure, Function, and Antigenicity of the SARS-CoV-2 Spike Glycoprotein,” *Cell*, vol. 181, no. 2, pp. 281-292.e6, Apr. 2020, doi: 10.1016/j.cell.2020.02.058.

[19] J. A. Jaimes, N. M. André, J. S. Chappie, J. K. Millet, and G. R. Whittaker, “Phylogenetic Analysis and Structural Modeling of SARS-CoV-2 Spike Protein Reveals an Evolutionary Distinct and Proteolytically Sensitive Activation Loop,” *J. Mol. Biol.*, vol. 432, no. 10, pp. 3309–3325, May 2020, doi: 10.1016/j.jmb.2020.04.009.

[20] Y. Huang, C. Yang, X. feng Xu, W. Xu, and S. wen Liu, “Structural and functional properties of SARS-CoV-2 spike protein: potential antivirus drug development for COVID-19,” *Acta Pharmacologica Sinica*, vol. 41, no. 9. Springer Nature, pp. 1141–1149, Sep. 01, 2020, doi: 10.1038/s41401-020-0485-4.

[21] J. A. Jaimes, N. M. André, J. S. Chappie, J. K. Millet, and G. R. Whittaker, “Phylogenetic Analysis and Structural Modeling of SARS-CoV-2 Spike Protein Reveals an Evolutionary Distinct and Proteolytically Sensitive Activation Loop,” *J. Mol. Biol.*, vol. 432, no. 10, pp. 3309–3325, May 2020, doi: 10.1016/j.jmb.2020.04.009.

[22] D. Kim, J. Y. Lee, J. S. Yang, J. W. Kim, V. N. Kim, and H. Chang, “The Architecture of SARS-CoV-2 Transcriptome,” *Cell*, vol. 181, no. 4, pp. 914-921.e10, May 2020, doi: 10.1016/j.cell.2020.04.011.

[23] A. A. T. Naqvi *et al.*, “Insights into SARS-CoV-2 genome, structure, evolution, pathogenesis and therapies: Structural genomics approach,” *Biochim. Biophys. Acta - Mol. Basis Dis.*, vol. 1866, no. 10, p. 165878, 2020, doi: 10.1016/j.bbadis.2020.165878.

[24] N. Chen *et al.*, “Epidemiological and clinical characteristics of 99 cases of 2019 novel coronavirus pneumonia in Wuhan, China: a descriptive study,” *Lancet*, vol. 395, no. 10223, pp. 507–513, Feb. 2020, doi: 10.1016/S0140-6736(20)30211-7.

[25] T. Gao *et al.*, “Identification and functional analysis of the SARS-COV-2 nucleocapsid protein,” *BMC Microbiol.*, vol. 21, no. 1, p. 58, Dec. 2021, doi: 10.1186/s12866-021-02107-3.

[26] B. W. Neuman *et al.*, “A structural analysis of M protein in coronavirus assembly and morphology,” *J. Struct. Biol.*, vol. 174, no. 1, pp. 11–22, Apr. 2011, doi: 10.1016/j.jsb.2010.11.021.

[27] M. Rastogi, N. Pandey, A. Shukla, and S. K. Singh, “SARS coronavirus 2: from genome to infectome,” *Respiratory Research*, vol. 21, no. 1. BioMed Central Ltd, pp. 1–15, Dec. 01, 2020, doi: 10.1186/s12931-020-01581-z.

[28] F. De Maio *et al.*, “Improved binding of SARS-CoV-2 Envelope protein to tight junction-associated PALS1 could play a key role in COVID-19 pathogenesis,” *Microbes Infect.*, vol. 22, no. 10, pp. 592–597, Nov. 2020, doi: 10.1016/j.micinf.2020.08.006.

[29] J. Shang *et al.*, “Structural basis of receptor recognition by SARS-CoV-2,” *Nature*, vol. 581, no. 7807, pp. 221–224, May 2020, doi: 10.1038/s41586-020-2179-y.

[30] J. Lan *et al.*, “Structure of the SARS-CoV-2 spike receptor-binding domain bound to the ACE2 receptor,” *Nature*, vol. 581, no. 7807, pp. 215–220, May 2020, doi: 10.1038/s41586-020-2180-5.

[31] C. Yi *et al.*, “Key residues of the receptor binding motif in the spike protein of SARS-CoV-2 that interact with ACE2 and neutralizing antibodies,” *Cell. Mol. Immunol.*, vol. 17, no. 6, pp. 621–630, Jun. 2020, doi: 10.1038/s41423-020-0458-z.

[32] J. Shang *et al.*, “Cell entry mechanisms of SARS-CoV-2,” *Proc. Natl. Acad. Sci. U. S. A.*, vol. 117, no. 21, pp. 11727–11734, May 2020, doi: 10.1073/pnas.2003138117.

[33] D. Wrapp *et al.*, “Cryo-EM structure of the 2019-nCoV spike in the prefusion conformation,” 2019. Accessed: Mar. 04, 2021. [Online]. Available: http://science.sciencemag.org/.

[34] M. Kosuge, E. Furusawa-Nishii, K. Ito, Y. Saito, and K. Ogasawara, “Point mutation bias in SARS-CoV-2 variants results in increased ability to stimulate inflammatory responses,” *Sci. Rep.*, vol. 10, no. 1, pp. 1–9, Dec. 2020, doi: 10.1038/s41598-020-74843-x.

[35] M. Cevik, K. Kuppalli, J. Kindrachuk, and M. Peiris, “Virology, transmission, and pathogenesis of SARS-CoV-2,” *BMJ*, vol. 371, Oct. 2020, doi: 10.1136/bmj.m3862.

[36] J. R. Larsen, M. R. Martin, J. D. Martin, P. Kuhn, and J. B. Hicks, “Modeling the Onset of Symptoms of COVID-19,” *Front. Public Heal.*, vol. 8, p. 473, Aug. 2020, doi: 10.3389/fpubh.2020.00473.

[37] I. Hamming, W. Timens, M. L. C. Bulthuis, A. T. Lely, G. J. Navis, and H. van Goor, “Tissue distribution of ACE2 protein, the functional receptor for SARS coronavirus. A first step in understanding SARS pathogenesis,” *J. Pathol.*, vol. 203, no. 2, pp. 631–637, Jun. 2004, doi: 10.1002/path.1570.

[38] B. Coutard, C. Valle, X. de Lamballerie, B. Canard, N. G. Seidah, and E. Decroly, “The spike glycoprotein of the new coronavirus 2019-nCoV contains a furin-like cleavage site absent in CoV of the same clade,” *Antiviral Res.*, vol. 176, p. 104742, Apr. 2020, doi: 10.1016/j.antiviral.2020.104742.

[39] D. Bestle *et al.*, “TMPRSS2 and furin are both essential for proteolytic activation and spread of SARS-CoV-2 in human airway epithelial cells and provide promising drug targets,” *bioRxiv*. bioRxiv, Apr. 15, 2020, doi: 10.1101/2020.04.15.042085.

[40] Y. Gao *et al.*, “Structure of the RNA-dependent RNA polymerase from COVID-19 virus,” *Science (80-.).*, vol. 368, no. 6492, pp. 779–782, May 2020, doi: 10.1126/science.abb7498.

[41] H. Kato *et al.*, “Length-dependent recognition of double-stranded ribonucleic acids by retinoic acid-inducible gene-I and melanoma differentiation-associated gene 5,” *J. Exp. Med.*, vol. 205, no. 7, pp. 1601–1610, Jul. 2008, doi: 10.1084/jem.20080091.

[42] T. Nelemans and M. Kikkert, “Viral innate immune evasion and the pathogenesis of emerging RNA virus infections,” *Viruses*, vol. 11, no. 10. MDPI AG, p. 961, Oct. 18, 2019, doi: 10.3390/v11100961.

[43] W. M. Schneider, M. D. Chevillotte, and C. M. Rice, “Interferon-stimulated genes: A complex web of host defenses,” *Annu. Rev. Immunol.*, vol. 32, pp. 513–545, 2014, doi: 10.1146/annurev-immunol-032713-120231.

[44] I.-Y. Chen, M. Moriyama, M.-F. Chang, and T. Ichinohe, “Severe Acute Respiratory Syndrome Coronavirus Viroporin 3a Activates the NLRP3 Inflammasome,” *Front. Microbiol.*, vol. 10, no. JAN, p. 50, Jan. 2019, doi: 10.3389/fmicb.2019.00050.

[45] J. Li *et al.*, “Virus-Host Interactome and Proteomic Survey Reveal Potential Virulence Factors Influencing SARS-CoV-2 Pathogenesis,” *Med*, vol. 2, no. 1, pp. 99-112.e7, Jan. 2021, doi: 10.1016/j.medj.2020.07.002.

[46] C. Huang *et al.*, “Clinical features of patients infected with 2019 novel coronavirus in Wuhan, China,” *Lancet*, vol. 395, no. 10223, pp. 497–506, Feb. 2020, doi: 10.1016/S0140-6736(20)30183-5.

[47] A. Grifoni *et al.*, “Targets of T Cell Responses to SARS-CoV-2 Coronavirus in Humans with COVID-19 Disease and Unexposed Individuals,” *Cell*, vol. 181, no. 7, pp. 1489-1501.e15, Jun. 2020, doi: 10.1016/j.cell.2020.05.015.

[48] K. G. Lokugamage *et al.*, “Type I Interferon Susceptibility Distinguishes SARS-CoV-2 from SARS-CoV,” *J. Virol.*, vol. 94, no. 23, pp. 1410–1430, Sep. 2020, doi: 10.1128/jvi.01410-20.

[49] J. Braun *et al.*, “SARS-CoV-2-reactive T cells in healthy donors and patients with COVID-19,” *Nature*, vol. 587, no. 7833, pp. 270–274, Nov. 2020, doi: 10.1038/s41586-020-2598-9.

[50] Invivogen, “Predicted immune responses to SARS-CoV-2,” *Invivogen Rev.*, vol. 33, no. 0, pp. 19–20, 2020.

[51] A. Zeltins, “Construction and characterization of virus-like particles: A review,” *Molecular Biotechnology*, vol. 53, no. 1. Nature Publishing Group, pp. 92–107, Jan. 2013, doi: 10.1007/s12033-012-9598-4.

[52] D. Yan, Y. Q. Wei, H. C. Guo, and S. Q. Sun, “The application of virus-like particles as vaccines and biological vehicles,” *Applied Microbiology and Biotechnology*, vol. 99, no. 24. Springer Verlag, pp. 10415–10432, Dec. 01, 2015, doi: 10.1007/s00253-015-7000-8.

[53] B. Schwarz, M. Uchida, and T. Douglas, Biomedical and Catalytic Opportunities of Virus-Like Particles in Nanotechnology, 1st ed., vol. 97. Elsevier Inc., 2017.

[54] L. A. Lee, Z. Niu, and Q. Wang, “Viruses and virus-like protein assemblies-Chemically programmable nanoscale building blocks,” Nano Res., vol. 2, no. 5, pp. 349–364, 2009, doi: 10.1007/s12274-009-9033-8.

[55] K. D. Brune et al., “Plug-and-Display: decoration of Virus-Like Particles via isopeptide bonds for modular immunization,” Sci. Rep., vol. 6, no. 1, pp. 1–13, Jan. 2016, doi: 10.1038/srep19234.

[56] A. Jegerlehner et al., “A molecular assembly system that renders antigens of choice highly repetitive for induction of protective B cell responses,” *Vaccine*, vol. 20, no. 25–26, pp. 3104–3112, 2002, doi: 10.1016/S0264-410X(02)00266-9.

[57] T. Koho et al., “His-tagged norovirus-like particles: A versatile platform for cellular delivery and surface display,” Eur. J. Pharm. Biopharm., vol. 96, pp. 22–31, 2015, doi: 10.1016/j.ejpb.2015.07.002.

[58] K. G. Patel and J. R. Swartz, “Surface functionalization of virus-like particles by direct conjugation using azide-alkyne click chemistry,” Bioconjug. Chem., vol. 22, no. 3, pp. 376–387, Mar. 2011, doi: 10.1021/bc100367u.

[59] B. Zakeri *et al.*, “Peptide tag forming a rapid covalent bond to a protein, through engineering a bacterial adhesin,” *Proc. Natl. Acad. Sci. U. S. A.*, vol. 109, no. 12, pp. E690–E697, Mar. 2012, doi: 10.1073/pnas.1115485109.

[60] D. Hatlem, T. Trunk, D. Linke, and J. C. Leo, “Catching a SPY: Using the SpyCatcher-SpyTag and related systems for labeling and localizing bacterial proteins,” *Int. J. Mol. Sci.*, vol. 20, no. 9, May 2019, doi: 10.3390/ijms20092129.

[61] S. Thrane *et al.*, “Bacterial superglue enables easy development of efficient virus-like particle based vaccines,” *J. Nanobiotechnology*, vol. 14, no. 1, p. 30, Apr. 2016, doi: 10.1186/s12951-016-0181-1.

[62] R. Rahikainen *et al.*, “Overcoming Symmetry Mismatch in Vaccine Nanoassembly through Spontaneous Amidation,” *Angew. Chemie Int. Ed.*, vol. 60, no. 1, pp. 321–330, Jan. 2021, doi: 10.1002/anie.202009663.

[63] C. M. Buldun, I. N. A. Khairil Anuar, and M. Howarth, “Snoopligase-mediated peptide–peptide conjugation and purification,” *Methods Mol. Biol.*, vol. 2208, pp. 13–31, 2021, doi: 10.1007/978-1-0716-0928-6_2.

[64] J. O. Fierer, G. Veggiani, and M. Howarth, “SpyLigase peptide-peptide ligation polymerizes affibodies to enhance magnetic cancer cell capture,” *Proc. Natl. Acad. Sci. U. S. A.*, vol. 111, no. 13, p. E1176, Apr. 2014, doi: 10.1073/pnas.1315776111.

[65] C. Qian *et al.*, “Recent progress on the versatility of virus-like particles,” *Vaccines*, vol. 8, no. 1. MDPI AG, p. 139, Mar. 01, 2020, doi: 10.3390/vaccines8010139.

[66] D. M. Da Silva, S. C. Fausch, J. S. Verbeek, and W. M. Kast, “Uptake of Human Papillomavirus Virus-Like Particles by Dendritic Cells Is Mediated by Fcγ Receptors and Contributes to Acquisition of T Cell Immunity,” *J. Immunol.*, vol. 178, no. 12, pp. 7587–7597, Jun. 2007, doi: 10.4049/jimmunol.178.12.7587.

[67] M. P. Rudolf, S. C. Fausch, D. M. Da Silva, and W. M. Kast, “Human Dendritic Cells Are Activated by Chimeric Human Papillomavirus Type-16 Virus-Like Particles and Induce Epitope-Specific Human T Cell Responses In Vitro,” *J. Immunol.*, vol. 166, no. 10, pp. 5917–5924, May 2001, doi: 10.4049/jimmunol.166.10.5917.

[68] J. Bessa *et al.*, “Low-affinity B cells transport viral particles from the lung to the spleen to initiate antibody responses,” *Proc. Natl. Acad. Sci. U. S. A.*, vol. 109, no. 50, pp. 20566–20571, Dec. 2012, doi: 10.1073/pnas.1206970109.

[69] R. L. Atmar and M. K. Estes, “The Epidemiologic and Clinical Importance of Norovirus Infection,” *Gastroenterology Clinics of North America*, vol. 35, no. 2. Gastroenterol Clin North Am, pp. 275–290, Jun. 2006, doi: 10.1016/j.gtc.2006.03.001.

[70] T. Koho *et al.*, “Production and characterization of virus-like particles and the P domain protein of GII.4 norovirus,” *J. Virol. Methods*, vol. 179, no. 1, pp. 1–7, 2012, doi: 10.1016/j.jviromet.2011.05.009.

[71] T. Koho *et al.*, “Purification of norovirus-like particles (VLPs) by ion exchange chromatography,” *J. Virol. Methods*, vol. 181, no. 1, pp. 6–11, 2012, doi: 10.1016/j.jviromet.2012.01.003.

[72] V. Lampinen, “Development of antigen-decorated norovirus-like particles for vaccine applications Pro Gradu -tutkielma,” no. April, 2018.

[73] B. Greenwood, “The contribution of vaccination to global health: Past, present and future,” *Philosophical Transactions of the Royal Society B: Biological Sciences*, vol. 369, no. 1645. Royal Society of London, Jun. 19, 2014, doi: 10.1098/rstb.2013.0433.

[74] J. H. Kim, F. Marks, and J. D. Clemens, “Looking beyond COVID-19 vaccine phase 3 trials,” *Nature Medicine*, vol. 27, no. 2. Nature Research, pp. 205–211, Feb. 01, 2021, doi: 10.1038/s41591-021-01230-y.

[75] D. Y. Logunov *et al.*, “Safety and efficacy of an rAd26 and rAd5 vector-based heterologous prime-boost COVID-19 vaccine: an interim analysis of a randomised controlled phase 3 trial in Russia,” *Lancet*, vol. 397, no. 10275, pp. 671–681, Feb. 2021, doi: 10.1016/s0140-6736(21)00234-8.

[76] F. P. Polack *et al.*, “Safety and Efficacy of the BNT162b2 mRNA Covid-19 Vaccine,” *N. Engl. J. Med.*, vol. 383, no. 27, pp. 2603–2615, Dec. 2020, doi: 10.1056/NEJMoa2034577.

[77] L. R. Baden *et al.*, “Efficacy and Safety of the mRNA-1273 SARS-CoV-2 Vaccine,” *N. Engl. J. Med.*, vol. 384, no. 5, pp. 403–416, Feb. 2021, doi: 10.1056/nejmoa2035389.

[78] M. Voysey *et al.*, “Safety and efficacy of the ChAdOx1 nCoV-19 vaccine (AZD1222) against SARS-CoV-2: an interim analysis of four randomised controlled trials in Brazil, South Africa, and the UK,” *Lancet*, vol. 397, no. 10269, pp. 99–111, Jan. 2021, doi: 10.1016/S0140-6736(20)32661-1.

[79] J. Sadoff *et al.*, “Interim Results of a Phase 1–2a Trial of Ad26.COV2.S Covid-19 Vaccine,” *N. Engl. J. Med.*, p. NEJMoa2034201, Jan. 2021, doi: 10.1056/NEJMoa2034201.

[80] M. Dan *et al.*, “Immunological memory to SARS-CoV-2 assessed for up to 8 months after infection,” *Science (80-.).*, vol. 371, no. 6529, Feb. 2021, doi: 10.1126/science.abf4063.

[81] L. B. Rodda *et al.*, “Functional SARS-CoV-2-Specific Immune Memory Persists after Mild COVID-19,” *Cell*, vol. 184, no. 1, pp. 169-183.e17, Jan. 2021, doi: 10.1016/j.cell.2020.11.029.

[82] “Science Brief: Emerging SARS-CoV-2 Variants | CDC.” https://www.cdc.gov/coronavirus/2019-ncov/more/science-and-research/scientific-brief-emerging-variants.html (accessed Mar. 06, 2021).

[83] “Stain-Free Imaging Technology | LSR | Bio-Rad.” https://www.bio-rad.com/en-fi/applications-technologies/stain-free-imaging-technology?ID=NZ0G1815 (accessed Feb. 10, 2021).

[84] “5-FAM (5-Carboxyfluorescein), Amine-reactive fluorescent label (CAS 76823-03-5) (ab145293).” https://www.abcam.com/5-fam-5-carboxyfluorescein-amine-reactive-fluorescent-label-ab145293.html (accessed Feb. 10, 2021).

[85] J. A. Bornhorst and J. J. Falke, “Purification of proteins using polyhistidine affinity tags,” *Methods in Enzymology*, vol. 326. Academic Press Inc., pp. 245–254, 2000, doi: 10.1016/s0076-6879(00)26058-8.

[86] O. Bahadir, “Ion-Exchange Chromatography and Its Applications,” in *Column Chromatography*, InTech, 2013.

[87] “pOET5 Transfer PlasmidOxford Expression Technologies.” https://oetltd.com/product/poet5-transfer-plasmid/ (accessed Feb. 02, 2021).

[88] O. Expression, G. L. Campus, and C. Information, “baculoFECTIN II USER GUIDE,” vol. 44, no. 0, pp. 1–2, 1865.

[89] Clontech, “BacPAK ™ Baculovirus Rapid Titer Kit User Manual,” *Mol. Biol. Manuals*, vol. 1, no. 631406, pp. 1–13, 2008.

[90] “Addgene: pET28a-AviTag-SnoopLigase.” https://www.addgene.org/105626/ (accessed Feb. 03, 2021).

[91] A. S. Ampules, “Pierce BCA Protein Assay Kit,” vol. 0747, no. 23225, pp. 0–3, 2000.

[92] P. Biotechnology, “a35389,” vol. 0747, no. 2162632, pp. 0–3.

[93] M. Fairhead and M. Howarth, “Site-specific biotinylation of purified proteins using BirA,” *Methods Mol. Biol.*, vol. 1266, pp. 171–184, 2015, doi: 10.1007/978-1-4939-2272-7_12.

[94] N. V. V. Saarinen *et al.*, “Multiplexed high-throughput serological assay for human enteroviruses,” *Microorganisms*, vol. 8, no. 6, pp. 1–16, Jun. 2020, doi: 10.3390/microorganisms8060963.

[95] F. H. Niesen, H. Berglund, and M. Vedadi, “The use of differential scanning fluorimetry to detect ligand interactions that promote protein stability,” *Nat. Protoc.*, vol. 2, no. 9, pp. 2212–2221, 2007, doi: 10.1038/nprot.2007.321.

[96] D. Wang *et al.*, “Immunoinformatic analysis of T-and B-cell epitopes for SARS-CoV-2 vaccine design,” *Vaccines*, vol. 8, no. 3, pp. 1–15, 2020, doi: 10.3390/vaccines8030355.

[97] D. C. Tessier, D. Y. Thomas, H. E. Khouri, F. Laliberié, and T. Vernet, “Enhanced secretion from insect cells of a foreign protein fused to the honeybee melittin signal peptide,” *Gene*, vol. 98, no. 2, pp. 177–183, 1991, doi: 10.1016/0378-1119(91)90171-7.

[98] S. Kukkurainen *et al.*, “The F1 loop of the talin head domain acts as a gatekeeper in integrin activation and clustering,” *J. Cell Sci.*, vol. 133, no. 19, Oct. 2021, doi: 10.1242/jcs.239202.

[99] S. Ray *et al.*, “Neutralized chimeric avidin binding at a reference biosensor surface,” *Langmuir*, vol. 31, no. 6, pp. 1921–1930, Feb. 2015, doi: 10.1021/la503213f.

[100] M. Danaei *et al.*, “Impact of particle size and polydispersity index on the clinical applications of lipidic nanocarrier systems,” *Pharmaceutics*, vol. 10, no. 2, pp. 1–17, 2018, doi: 10.3390/pharmaceutics10020057.

[101] A. Note, “Application Note Glycosylation of the Receptor Binding Domain of Covid-19 Virus Spike Protein,” vol. 2019, pp. 19–22, 2020.

[102] Y. Zhang *et al.*, “Site-specific N-glycosylation Characterization of Recombinant SARS-CoV-2 Spike Proteins,” *Mol. Cell. Proteomics*, p. mcp.RA120.002295, Oct. 2020, doi: 10.1074/mcp.ra120.002295.

[103] T. K. Tan *et al.*, “A COVID-19 vaccine candidate using SpyCatcher multimerization of the SARS-CoV-2 spike protein receptor-binding domain induces potent neutralising antibody responses,” *Nat. Commun.*, vol. 12, no. 1, p. 542, Dec. 2021, doi: 10.1038/s41467-020-20654-7.

[104] Z. Roth, G. Yehezkel, and I. Khalaila, “Identification and Quantification of Protein Glycosylation,” *Int. J. Carbohydr. Chem.*, vol. 2012, pp. 1–10, Apr. 2012, doi: 10.1155/2012/640923.

[105] T. Li *et al.*, “SARS-CoV-2 spike produced in insect cells elicits high neutralization titres in non-human primates,” *Emerg. Microbes Infect.*, vol. 9, no. 1, pp. 2076–2090, Jan. 2020, doi: 10.1080/22221751.2020.1821583.

[106] S. F. Ahmed, A. A. Quadeer, and M. R. McKay, “Preliminary identification of potential vaccine targets for the COVID-19 Coronavirus (SARS-CoV-2) Based on SARS-CoV Immunological Studies,” *Viruses*, vol. 12, no. 3, 2020, doi: 10.3390/v12030254.

9. APPENDICES: AMINO ACID SEQUENCES OF DESIGNED PROTEINS

9.1 DogTag-noroVLP

DogTag-noroVLP (noro-VP1– SpeI– *linker* – DogTag)

```
MKMASSDANP  SDGSAANLVP  EVNNEVMALE  PVVGAAIAAP  VAGQQNVIDP  WIRNNFVQAP  60
GGEFTVSPRN  APGEILWSAP  LGPDLNPYLS  HLARMYNGYA  GGFEVQVILA  GNAFTAGKVI  120
FAAVPPNFPT  EGLSPSQVTM  FPHIVVDVRQ  LEPVLIPLPD  VRNNFYHYNQ  SNDPTIKLIA  180
MLYTPLRANN  AGDDVFTVSC  RVLTRPSPDF  DFIFLVPPTV  ESRTKPFSVP  VLTVEEMTNS  240
RFPIPLEKLF  TGPSSAFVVQ  PQNGRCTTDG  VLLGTTQLSP  VNICTFRGDV  THITGSRNYT  300
MNLASQNWND  YDPTEEIPAP  LGTPDFVGKI  QGVLTQTTRT  DGSTRGHKAT  VYTGSADFAP  360
KLGRVQFETD  TDRDFEANQN  TKFTPVGVIQ  DGGTTHRNEP  QQWVLPSYSG  RNTHNVHLAP  420
AVAPTFPGEQ  LLFFRSTMPG  CSGYPNMDLD  CLLPQEWVQY  FYQEAAPAQS  DVALLRFVNP  480
DTGRVLFECK  LHKSGYVTVA  HTGQHDLVIP  PNGYFRFDSW  VNQFYTLAPM  GNGTGRRRAV  540
TSGGDIPATY EFTDGKHYIT NEPIPPK                                          560
```

9.2 SnoopTagJr-RBD

SnoopTagJr-RBD (HBM-HisTag-TEVsite-RBD-**KasI**-linker-**SnoopTagJr)**

```
MKFLVNVALV FMVVYISYIY AHHHHHHDYD IPTTENLYFQ RVQPTESIVR FPNITNLCPF 60
GEVFNATRFA SVYAWNRKRI SNCVADYSVL YNSASFSTFK CYGVSPTKLN DLCFTNVYAD 120
SFVIRGDEVR QIAPGQTGKI ADYNYKLPDD FTGCVIAWNS NNLDSKVGGN YNYLYRLFRK 180
SNLKPFERDI STEIYQAGST PCNGVEGFNC YFPLQSYGFQ PTNGVGYQPY RVVVLSFELL 240
HAPATVCGPK KSTNLVKNKC VNFGAGSGSK LGSIEFIKVN K                      280
```

9.3 SnoopTagJr-RBM

SnoopTagJr-RBM (RBM – SnoopTagJr)

```
GNYNYLYRLF RKSNLKPFKL GSIEFIKVNK
```